Article

Cell

A Constant Size Extension Drives Bacterial Cell Size Homeostasis

Manuel Campos,[1,2,5] Ivan V. Surovtsev,[1,2,5] Setsu Kato,[3,5] Ahmad Paintdakhi,[1,2] Bruno Beltran,[1,2,3,6] Sarah E. Ebmeier,[1,3] and Christine Jacobs-Wagner[1,2,3,4,*]

[1]Microbial Sciences Institute, Yale University, West Haven, CT 06516, USA
[2]Howard Hughes Medical Institute
[3]Department of Molecular, Cellular, and Developmental Biology
[4]Department of Microbial Pathogenesis, Yale Medical School
Yale University, New Haven, CT 06520, USA
[5]Co-first author
[6]Present address: Department of Mathematics, Louisiana State University, Baton Rouge, LA 70803, USA
*Correspondence: christine.jacobs-wagner@yale.edu
http://dx.doi.org/10.1016/j.cell.2014.11.022

SUMMARY

Cell size control is an intrinsic feature of the cell cycle. In bacteria, cell growth and division are thought to be coupled through a cell size threshold. Here, we provide direct experimental evidence disproving the critical size paradigm. Instead, we show through single-cell microscopy and modeling that the evolutionarily distant bacteria *Escherichia coli* and *Caulobacter crescentus* achieve cell size homeostasis by growing, on average, the same amount between divisions, irrespective of cell length at birth. This simple mechanism provides a remarkably robust cell size control without the need of being precise, abating size deviations exponentially within a few generations. This size homeostasis mechanism is broadly applicable for symmetric and asymmetric divisions, as well as for different growth rates. Furthermore, our data suggest that constant size extension is implemented at or close to division. Altogether, our findings provide fundamentally distinct governing principles for cell size and cell-cycle control in bacteria.

INTRODUCTION

Cell size control, a universal property of all organisms, reflects the balance between growth and division. Mechanisms must be in place to ensure that cells narrowly distribute around a characteristic size for a given cell type, species, and growth condition. This is especially important for exponentially growing cells. Exponential growth implies that growth is proportional to cell size such that short cells grow slower than long cells in absolute growth rate. Thus, if no compensation occurs, any deviations from the mean size will increase cell size variability in the population at each generation. The very existence of a stable cell size distribution indicates the presence of intrinsic mechanisms that reduce cell size fluctuations.

Most cells—from bacteria to yeast to mammalian cells—are thought to regulate their size and cell cycle through critical size thresholds (Turner et al., 2012). In the critical size model, cells commit to division upon reaching a size threshold. Thus, all cells divide at about the same size whether they are born shorter or longer than the mean, compensating for their initial size deviation. The size threshold, or "sizer," can be applied to a cell-cycle event other than division, with completion of this earlier event licensing cell division to occur after a constant amount of time, or "timer," has elapsed. For example, the yeast *Saccharomyces cerevisiae* and *Schizosaccharomyces pombe* display a size threshold at the G1-S transition and mitosis, respectively (Fantes, 1977; Johnston et al., 1977; Sveiczer et al., 1996). In the bacterial field, a "sizer + timer" model gained momentum with seminal population studies in *Escherichia coli* and *Salmonella typhimurium*. A size threshold at the initiation of DNA replication was inferred from calculations showing that, on average, DNA replication initiates at a constant cell mass under different growth rate conditions (Donachie, 1968). Although disputed (Bates and Kleckner, 2005; Boye and Nordström, 2003; Wold et al., 1994), a coupling of cell division to DNA replication through a fixed timer was suggested from experiments showing that the timing between DNA replication and cell division remains constant across different growth rates (Cooper and Helmstetter, 1968; Schaechter et al., 1958; Schaechter et al., 1962). These findings observed at the population level were then assumed to be applicable to individual cells.

Cell size homeostasis could, at least in theory, be achieved through mechanisms that do not involve the licensing of division upon attainment of a certain size. These alternative mechanisms include a molecular clock, a simple timer, the addition of a constant cell volume, transition probability, or a concerted "sloppy" sizer and timer (Fantes and Nurse, 1981; Osella et al., 2014). For example, based on mathematical modeling, Voorn and Koppes first (Voorn and Koppes, 1998), and Amir later (Amir, 2014) argued that addition of a constant volume at each generation can describe the experimental shape of bacterial cell size distributions as well as population-derived bulk correlations (the positive correlation in size between mothers and daughters and the negative correlation between cell-cycle time and size at birth). However, these statistical features have alternative explanations

(Hosoda et al., 2011; Osella et al., 2014) and can be described by sizer-based homeostasis mechanisms (Koch and Schaechter, 1962; Koppes et al., 1980; Robert et al., 2014; Turner et al., 2012). The concept of sizer-based control has prevailed in the bacterial literature and, apart from the exception of *Mycobacterium* (Santi et al., 2013), still persists today as an underlying assumption in virtually all bacterial cell size and cell-cycle studies.

Importantly, beyond their associated caveats, all bacterial cell size homeostasis models—including the prevalent sizer-based models—lack direct experimental evidence. A direct examination of an intrinsic cell size mechanism requires the ability to track a large number of individual cells. Cell tracking must occur in the absence of environmentally induced cell size fluctuations. This is important because *E. coli* and other bacteria traditionally used for cell size studies change their average size in response to nutrient availability and cell density (Akerlund et al., 1995; Schaechter et al., 1958). Finally, cell size must be measured with high precision and at high temporal resolution, preferably over multiple cell cycles.

Another overlooked aspect of bacterial cell size homeostasis is the role of division site placement. Most bacterial cell size studies—whether experimental or theoretical—have focused on symmetrically dividing bacteria, even though asymmetric divisions are well represented in the bacterial world. For example, the large class of α-proteobacteria appears to be dominated by asymmetrically dividing bacterial species. The best-studied α-proteobacterium is *Caulobacter crescentus*, which divides asymmetrically to produce two daughter cells of unequal sizes, known as the stalked and swarmer cells (Figure 1A).

In this study, we performed high-precision single-cell time-lapse microscopy studies on *C. crescentus* and *E. coli* to uncover the intrinsic principles of bacterial cell size homeostasis for both symmetric and asymmetric divisions.

RESULTS AND DISCUSSION

C. crescentus Does Not Appear to Vary Its Cell Length in Response to Changes in Nutrient Availability, Cell Density, or Temperature

In this study, we focused on cell length, as this is the cell size dimension that changes during the cell cycle. Cell length in bacteria is generally thought to be sensitive to environmental conditions. For example, *E. coli* and other bacteria are known to modulate their average length in response to nutrient availability and cell density (Akerlund et al., 1995; Schaechter et al., 1958). Using high-precision image analysis software (Sliusarenko et al., 2011), we found that, although the cell width slightly varies (Harris et al., 2014), the length of asymmetrically dividing *C. crescentus* appears insensitive to environmental fluctuations. There was no discernable difference in cell length distributions between *C. crescentus* populations grown in nutrient-poor (M2G) or nutrient-rich (PYE) medium (Figure 1B) despite significant differences in growth rates, with doubling times of 146 ± 5 min in M2G (mean ± SD, n = 2 experiments) and 96 ± 1 min in PYE (n = 2). Varying cell density (OD_{660nm} < 0.3 versus > 0.8) or temperature (25°C versus 30°C) also had little effect on cell length distributions (Figure 1B). These distributions were reproducible from day to day (data not shown). Thus, *C. crescentus* populations exhibited the same cell length distributions under all growth conditions tested, indicating robust cell length homeostasis. This allowed us to examine the intrinsic properties of cell length control, without concern of interference from environmental fluctuations.

C. crescentus Controls Its Cell Length

Studying cell length control requires precise measurements of cell length over at least one full cell cycle. Obtaining swarmer cells in G1 phase is relatively easy (Evinger and Agabian, 1979). However, the synchronization technique does not distinguish between the "young" swarmer cells that are fresh from division and the "older" swarmer cells that are about to become stalked cells. Furthermore, the technique, like most cell-cycle synchronization methods, perturbs cellular metabolism. Therefore, we performed time-lapse phase contrast microscopy of asynchronous populations and monitored growth and division (see Experimental Procedures). Analysis showed that, when cells were spotted on regular 1% agarose pads containing M2G medium, the average cell length became significantly shorter (~10%) even after a single cell cycle. We reasoned that this cell shortening was likely caused by physical constraints due to immobilization on the solid agarose (1%) substrate. To reduce this potential "sticky" problem, we spotted cells on soft agarose (0.3%) pads. In this more aqueous environment, cells were more loosely immobilized, allowing newborn swarmer cells to swim away immediately after their physical separation from the stalked cell sibling following division (Movie S1 available online). This soft-agarose microscopy set-up allowed us to track stalked cells over time and to measure their length from birth (*Lb*) to division (*Ld*). In this environment, the cell lengths remained similar between divisions, with cell length at birth *Lb* = 2.43 ± 0.39 μm (mean ± SD, n = 252 cells) after the first division versus *Lb* = 2.42 ± 0.40 μm (n = 193 cells) after the second division. Because swarmer cells occasionally became immobilized on the soft-agarose surface after a short swim (Movie S1), we also obtained measurements for swarmer cells, although many fewer (see Experimental Procedures).

As expected (Terrana and Newton, 1975), division was asymmetric, with a division ratio *DR* (length between the stalked pole and the division site divided by the total length) of 0.56 ± 0.04 (n = 706 cells) (Figure 1C). The populations of newborn stalked and swarmer cells were characterized by narrow distributions of cell length at birth (Figure 1D). Both cell types had a very similar relative variability in length, as measured by the coefficients of variation (CV, standard deviation/mean) of 16% and 18% for stalked and swarmer cells, respectively. Despite the shift in average length at birth, swarmer and stalked cells displayed similar distributions of cell lengths at division, indicating that swarmer cells must grow more than stalked cells to compensate for their shorter size at birth. The cell length distributions at division were narrow, with a CV of about 12% (Figure 1D). This value is comparable to the CV determined for *Saccharomyces cerevisiae* at budding (CV = 17%) and *Schizosaccharomyces pombe* at fission (CV = 6%) (Di Talia et al., 2007; Lord and Wheals, 1981; Sveiczer et al., 1996), both of which are known to display cell size regulation.

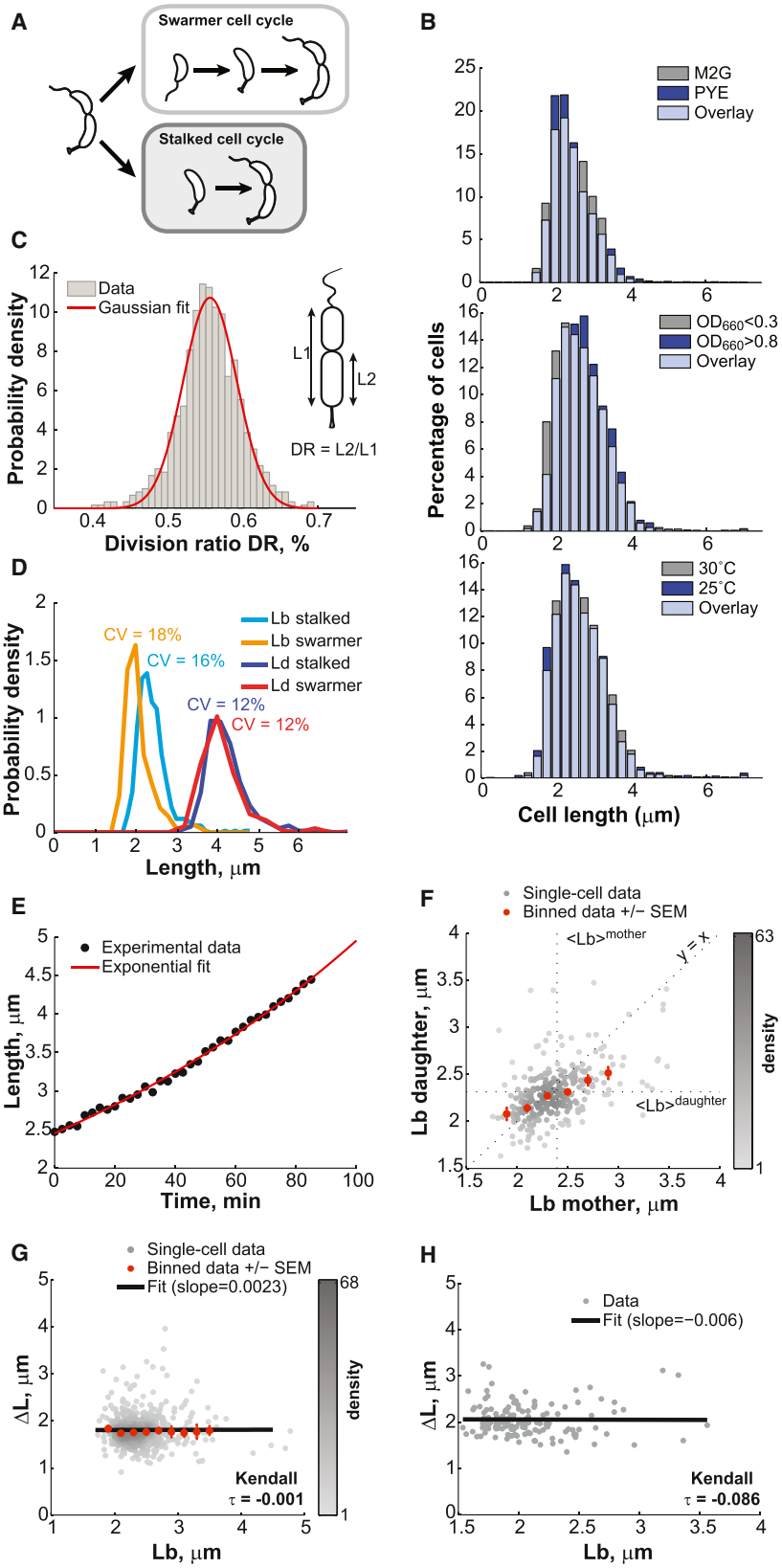

Figure 1. Cell Length Control in *C. crescentus*

(A) Schematic of the dimorphic cell cycle of *C. crescentus*. Each division generates two different progeny: the smaller swarmer cell and the longer stalked cell. The swarmer cell is motile thanks to a polar flagellum until the cell transitions to a stalked cell.

(B) Distribution of *C. crescentus* CB15N lengths under different environmental conditions. Cells were grown in M2G at 30°C and were imaged on 1% agarose pads at an OD_{660nm} < 0.3 except if stated otherwise.

(C) Histogram representing the distribution of the division ratio *DR* for *C. crescentus* CB15N cells (n = 706) grown in M2G medium and imaged on 0.3% agarose pads.

(D) Distribution of cell length at birth *Lb* and at division *Ld* for stalked cells (n = 565) and swarmer cells (n = 141) grown in M2G medium at 30°C and imaged at OD_{660nm} < 0.3 on 0.3% agarose pads. The coefficient of variation (SD/mean) for each distribution is shown.

(E) Representative growth curve of a single stalked cell (black circles) grown in M2G medium at 30°C on a 0.3% agar pad. The red line is the best fit of the data with an exponential function.

(F) Partial inheritance of *Lb* from one generation to the next (n = 457 stalked cells). The vertical and horizontal dotted lines indicate the mean length at birth for mother and daughter cells. The line y = x is also plotted for comparison purposes.

(G) Dependence of the elongation over a cell cycle (ΔL) on *Lb* for stalked cells. Gray dots represent single-cell data, whereas orange dots represent the average of binned data ± SEM. The shade of gray represents the density of points in a given area of the graph. The black line represents the linear fit to the single-cell data.

(H) Dependence of ΔL on *Lb* for swarmer cells. There were not enough cells (n = 141) to bin the data.

See also Figures S5 and S7 and Movie S1.

Cell Size Compensation Is Partial over a Single Generation

Further analysis was primarily done on the stalked progeny, given their higher sample size. Their cell elongation was consistent with exponential growth (Figure 1E), as reported previously (Siegal-Gaskins and Crosson, 2008). Exponential growth implies that a cell size compensation mechanism must be at work to maintain the narrow cell length distributions that we observed. We indeed found that stalked cells born shorter than the population average produced stalked cells that were comparatively longer than their mothers (*Lb* of daughter > *Lb* of mother) (Figure 1F). The reverse was true for cells born longer than the mean; their progeny were comparatively shorter. However, the compensation was only partial (Figure 1F). This was surprising because a sizer-based model (with or without timer) implies that all cells shorter than the critical size grow until they reach their size threshold. As a result, there should not be any correlation in cell length between mothers and daughters for cells born shorter than the critical size. In other words, the "short" phenotype is not an inheritable feature when a critical size mechanism is in place, unlike what we observed.

C. crescentus Cells Elongate by a Constant Amount on Average, Irrespective of Cell Length at Birth

Another key characteristic of any sizer-based model is that cells born smaller than the mean size grow, on average, more before dividing than cells born longer. Thereby, in a sizer model, cell extension during the cell cycle (ΔL = *Ld*-*Lb*) displays a strong negative correlation with the cell length at birth (*Lb*) for cells born shorter than the critical size (Fantes, 1977; Sveiczer et al., 1996). Strikingly, we found no significant correlation (slope ~0, Kendall $\tau = -0.001$) between ΔL and *Lb* for stalked cells (n = 565, Figure 1G). This seemed to be also true for the swarmer progeny despite lower statistics (n = 141, Figure 1H). These data suggest that *C. crescentus* cells do not sense a certain size to regulate their length. Instead, they simply elongate the same amount on average (ΔL = 1.81 ± 0.36 μm and 2.06 ± 0.35 μm for stalked and swarmer progeny, respectively) before dividing, regardless of their size at birth.

E. coli Does Not Sense a Cell Size Threshold to Control Its Length

The surprising lack of cell size threshold in *C. crescentus* prompted us to revisit the critical size paradigm in *E. coli*, which had mostly been inferred from population studies under fast-growing conditions (Cooper, 1991; Cooper and Helmstetter, 1968; Donachie, 1968). Because the size of *E. coli* is sensitive to changes in nutrient availability or cell density, it was crucial to maintain constant growth conditions during measurements. For this, we used a microfluidic device (Ullman et al., 2013) that allowed us to track hundreds of *E. coli* BW25113 cells at the high temporal resolution of 5 s for hours (Figure S1 and Movie S2). We used fast-growth conditions (LB-rich medium at 30°C) that resulted in an interdivision time of 27 ± 5 min (mean ± SD, n = 1,305 cells). We verified that the growth rate and the average cell length at birth remained constant through the entire 7 hr experiment (Figures 2A and 2B), indicating steady-state conditions. We also verified that the position of the cells in the microfluidic chamber had no influence on these parameters (Figure S1B). Cell elongation at the single-cell level was well approximated with an exponential function (Figure 2C), consistent with exponential growth.

Cell lengths at birth and division were narrowly distributed, with low CV of 12% and 11% (Figure 2D), respectively, consistent with previous reports (Koppes et al., 1980; Wakamoto et al., 2005). Strikingly, *E. coli*, even under fast-growing conditions, behaved similarly to *C. crescentus* in many respects. First, cells born shorter or longer than the mean only displayed partial cell size compensation over a single cell cycle (Figure 2E). Second, there was no correlation between the amount of elongation over a cell cycle and the length of cells at birth (Figure 2F). *E. coli* cells grew, on average, the same length (ΔL = 3.23 ± 0.60 μm, mean ± SD, n = 1,305 cells) before dividing, independent of their initial size. These results demonstrate a fundamental conflict with the predictions of a sizer-based mechanism.

By analyzing published microfluidic data (Wang et al., 2010) (see Experimental Procedures), we found that ΔL is also independent of *Lb* for *E. coli* strains MG1655 and B/r growing at 37°C in 1 μm wide linear chambers (Figure S2), suggesting that our observations are independent from the strain, the microfluidic chamber geometry, and the temperature.

A Constant Cell Elongation per Cell Cycle Results in Cell Size Homeostasis

How can cells control their size in the absence of a sizer mechanism? Our data show that, although there are significant fluctuations in ΔL values, cells elongate, on average, a constant amount before dividing, irrespective of their length at birth (Figures 1G, 1H, 2F, and S2). A constant elongation —or the addition of a volume increment— can, at least theoretically, lead to cell size homeostasis (Amir, 2014; Voorn and Koppes, 1998). Figure 3A shows schematically how a constant length extension followed by a symmetric division can compensate for cell size fluctuations within a few generations. Mathematically (see Extended Experimental Procedures, Equation 3), cell lengths at birth that deviate from the mean converge exponentially over generations toward the constant elongation value in the absence of noise (Figure 3B). This assumes that all cells extend by the exact same increment ΔL, divide precisely in half, and grow at an identical relative rate α. In reality, these parameters fluctuate around an average value. When the experimental variability in ΔL, *DR*, and α was considered in our mathematical model, stochastic simulations (see Extended Experimental Procedures) showed that virtual newborn cells of varying initial lengths (1–10 μm) converge to the expected steady-state distribution of *Lb* within two to four divisions (Figure 3C). After that, *Lb* fluctuates around the average value (Figure 3D) and the population as a whole reaches a steady-state regime in which the *Lb* distribution remains stable over time (Figure 3E). Thus, the constant extension mechanism does not need to be precise to be robust.

Remarkably, the steady-state distribution of *Lb* obtained from the simulations almost perfectly overlapped with the experimental distribution (Figure 3F), providing further support for the constant extension model. The model also quantitatively predicts the cell size compensation profile after one generation (Figure 3G compared to 2E), as well as over subsequent generations (Figure 3H compared to 3I). Because we were able to track cell

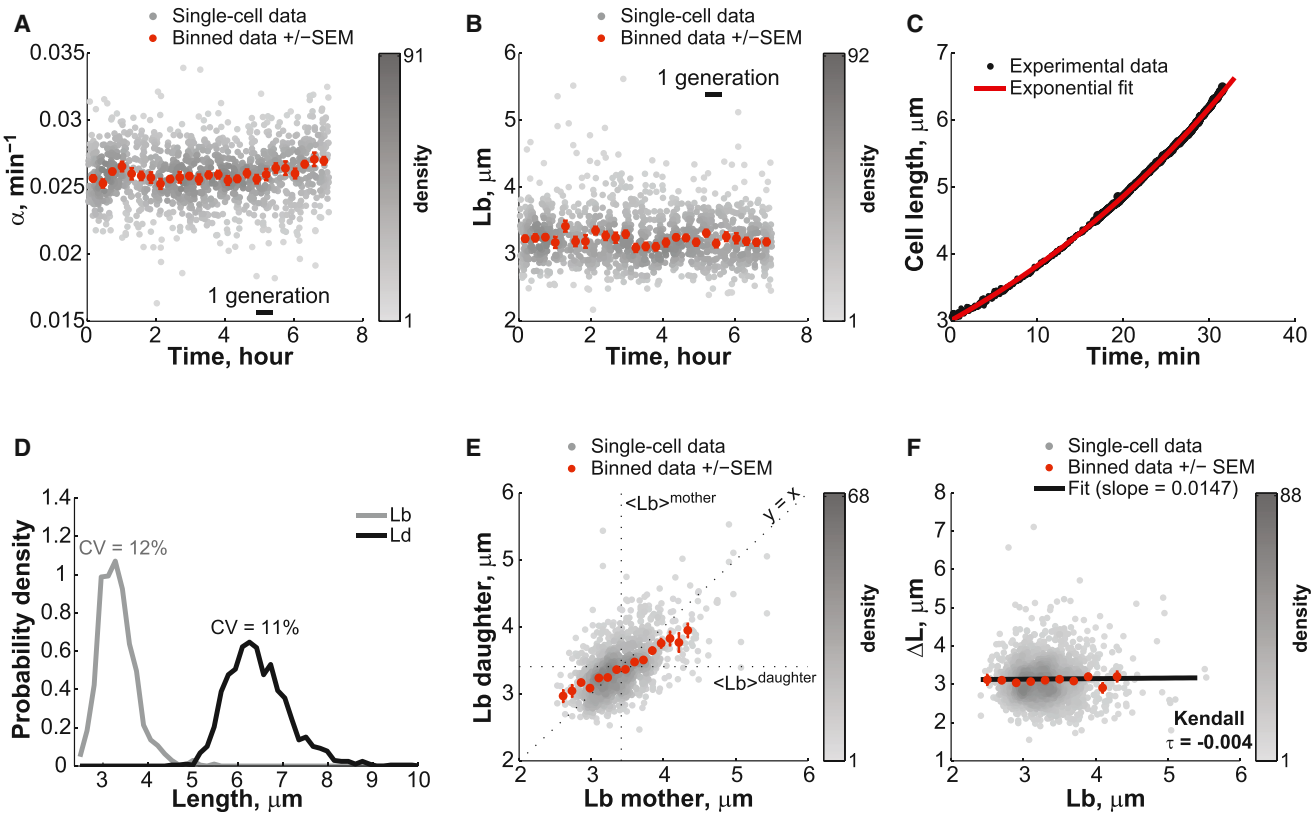

Figure 2. Steady-State Growth of *E. coli* BW25113 Cells in Microfluidic Chambers

E. coli BW25113 cells (n = 1,305) were grown in microfluidic chambers at 30°C in nutrient-rich LB medium.

(A) Relative growth rate α over the course of the > 7 hr long microfluidic experiment. Gray dots represent single-cell data, whereas orange dots represent the average of binned data ± SEM.

(B) Same as (A) except that *Lb* was plotted instead of α.

(C) Representative growth curve of a single cell (black circles). Length was measured every 5 s. The red line is the best fit of the data with an exponential function.

(D) Distribution of *Lb* and *Ld*.

(E) Partial inheritance of *Lb* from one generation to the next.

(F) Dependence of ΔL on *Lb*. The black line represents the linear fit to the single-cell data.

See also Figures S1, S2, S5, S7 and Movie S2.

lineages over several generations in our *E. coli* microfluidic experiments, we also showed that the correlation in *Lb* between ancestors and descendants drops with the number of generations (Figure 3J), following an exponential decay consistent with the constant extension model (see Extended Experimental Procedures, Equation 3). Thus, the model accurately predicts the degree of correlation in *Lb* between ancestors and descendants.

The constant extension model works equally well for asymmetric divisions. Using the experimental ΔL and *DR* values for the *C. crescentus* data set, simulations accurately reproduced the experimental *Lb* distribution of both stalked and swarmer daughter cells (Figure S3A). For symmetrically dividing bacteria (average division ratio $\langle DR \rangle = 0.5$), the average length at birth ($\langle Lb \rangle$) equals the average elongation ($\langle \Delta L \rangle$), as shown for *E. coli* (Figure S3B). For asymmetrically dividing bacteria, this is not the case (Figure S3C). $\langle \Delta L \rangle$ of the longer progeny will correspond to $\langle Lb \rangle$ of the smaller one and vice versa (see Extended Experimental Procedures, Equation 2). For example, the average length extension of *C. crescentus* stalked cells is, within the measurement error, equal to the length of swarmer cells at birth (Figure S3C).

Precision in Cell Length at Birth Is Dictated by the Division Ratio and the Length Extension between Divisions

Just as the average *Lb* value is determined by the average ΔL and *DR* values, deviations from this targeted size—which is reflected by the CV of the *Lb* distribution—will be dictated by the precision of both the constant extension mechanism and the positioning of the division machinery. Note that, although the average ΔL is equal to the average *Lb* for symmetrically dividing cells, variations in ΔL and *Lb* can be different (Figure S3B). The constant extension model (see Extended Experimental Procedures, Equations 14 and 15) quantitatively predicts how the CV of *Lb* depends on the CV of ΔL and *DR* (Figures S3D and S3E). We found that the predicted CV values of *Lb* are in excellent agreement with the experimental values (Figures S3D and S3E).

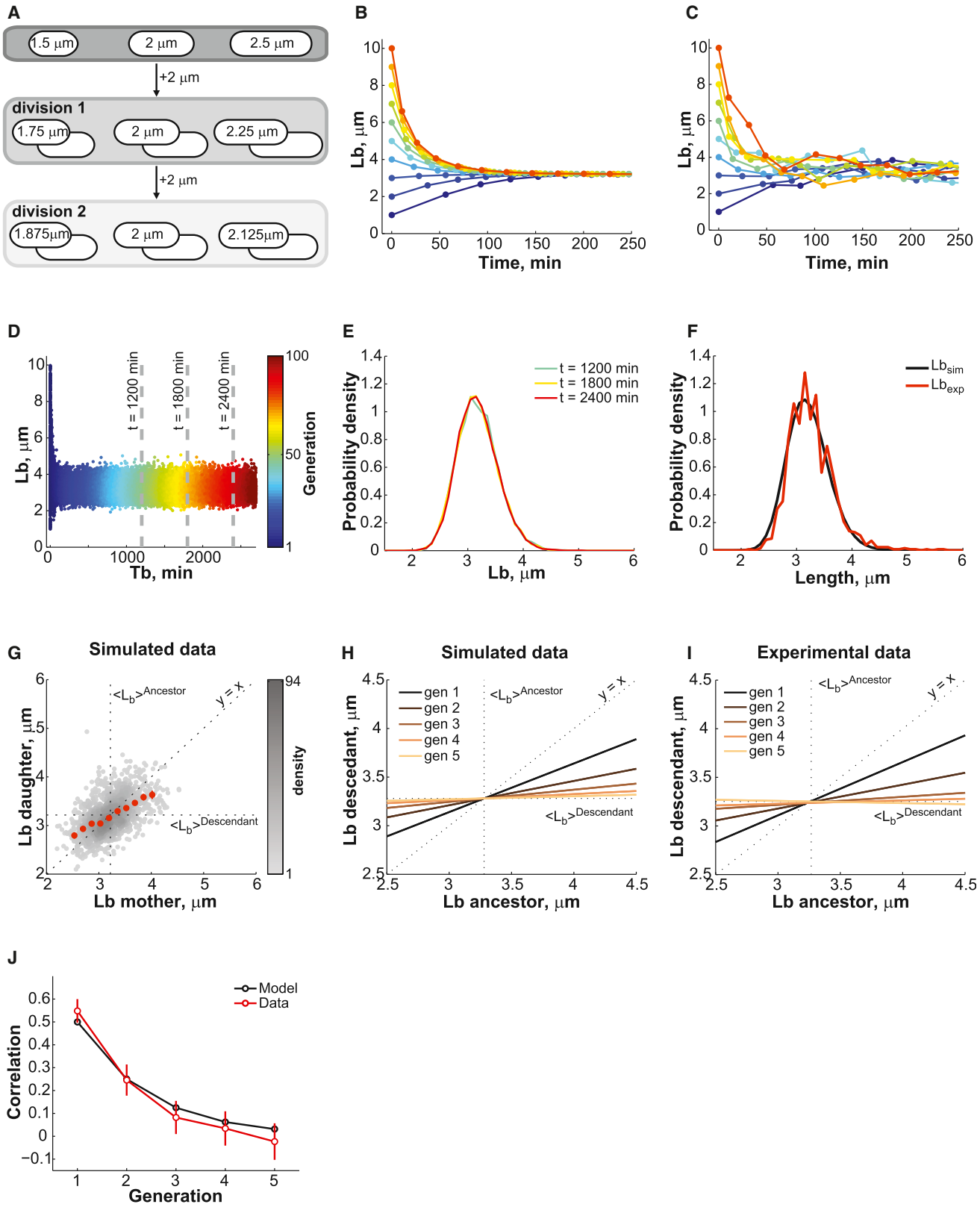

(legend on next page)

Cell-Cycle Time Increases with Shorter Cell Length at Birth

How do cells elongate by the same amount on average? Is it by modulating their cell-cycle time T or by changing their relative elongation rate α? We found that, for both the *E. coli* and *C. crescentus* data sets, T decreases as Lb increases (Figures 4A and 4B), whereas α remains fairly constant (Figures 4C and 4D), as previously reported for *E. coli* (Osella et al., 2014). Note that the *relative* elongation rate α (min^{-1}) corresponds to the relative length increase over time, not to be confused with the *absolute* elongation rate ($\mu m\ min^{-1}$), which is the absolute increase of cell length over a period of time. By virtue of their exponential growth, a constant relative elongation rate implies that the absolute elongation rate averaged over the cell cycle will increase with increasing Lb, which is what we observed (Figures 4C and 4D).

Collectively, our data show that cells modulate their cell-cycle time, and not their relative growth rate, to achieve the same length extension. As a result, the so-called "normalized cell-cycle time" αT is negatively dependent on Lb (Figures 4E and 4F). This negative dependence is often taken as supportive evidence for a sizer-based mechanism. The rationale for this is that, if a cell needs to reach a certain size before committing to division, shorter cells at birth require longer cell-cycle times. However, this negative dependence between αT and Lb is also expected from the constant extension model. In fact, if we used the average ΔL values obtained from the *E. coli* and *C. crescentus* stalked cell experiments (ΔL = 3.23 μm and ΔL = 1.81 μm, respectively), we found that the analytical expression derived from the constant extension model (see Extended Experimental Procedures, Equation 5) describes the averaged data very well (Figures 4E and 4F).

The Constant Length Extension between Divisions Changes with Nutrient Availability in *E. coli*

It is well known that *E. coli* changes its size in response to nutrient availability (Schaechter et al., 1958). If cell size homeostasis works through a constant elongation irrespective of the composition of the growth medium, we would expect the fixed cell length extension in nutrient-poor medium to be smaller than in the nutrient-rich LB medium, with the average ΔL value matching the average Lb value for each growth medium. To test this hypothesis, we grew *E. coli* BW25113 in microfluidic chambers with M9-supplemented medium (M9 salts supplemented with 0.1% casamino acids and 0.2% glucose) instead of LB medium. Under steady-growth conditions (Figure S4), the cell-cycle time in M9 supplemented medium was longer than in LB medium with T = 42 ± 12 min, and the cell lengths at birth and at division were shifted to lower values (Figure 5A), with Lb = 2.32 ± 0.38 μm and Ld = 4.59 ± 0.71 μm. Cell size control in M9 medium remains precise, with CV values of 17% and 15% for Lb and Ld, respectively.

Importantly, as in rich medium, the correlation for the length at birth between mothers and daughters was 0.5 (Figure 5B), as expected from the constant extension model. In addition, ΔL and Lb remained uncorrelated (Kendall τ = 0.03, Figure 5C). Curiously, we observed correlations between some parameters (α of daughter versus α of mother and ΔL versus α, Figures S5A and S5B) in the M9 data that were absent in the LB data set (Figures S5C and S5D); however, these correlations had no impact on cell size regulation (Figures 5D, S5E, and Extended Experimental Procedures). Consistent with our hypothesis, cells elongated by a shorter increment before division occurs, with ΔL = 2.26 ± 0.59 μm in M9-supplemented medium compared to 3.23 ± 0.6 μm in rich LB medium to set the corresponding length at birth. This suggests that cells modulate their average length by changing the average ΔL in response to changes in nutrient availability.

If the latter is true, we reasoned that mutants impaired in the transport of the carbon source from the environment may behave as if they were growing in a carbon-poor medium: cells would implement a smaller average ΔL while fully maintaining size homeostasis (i.e., similar $CV_{\Delta L}$ as wild-type). The phosphotransferase system (PTS) is involved in the efficient transport of sugars across the membrane. Deletion of genes encoding the core PTS components PtsH and PtsI in *E. coli* resulted in a reduced growth rate (>2-fold) and a visibly shorter cell morphology in glucose-containing M9 supplemented medium (Figures 5E and 5F). The Δ*ptsH* and Δ*ptsI* mutants were also slightly thinner (data not shown). Consistent with our expectation, quantitative analysis (see Extended Experimental Procedures) showed that

Figure 3. Cell Size Control by a Constant Extension Model

(A) Schematic showing how a constant elongation allows cells of below- and above-average length to recover over time and generations.

(B) Analytical dependence of Lb on time for ten cells with Lb ranging from 1 to 10 μm. The time between data points represents the cell cycle (generation) time for that particular cell. See Table S1 for input parameter values.

(C) Same as (B) except that the experimentally observed fluctuations around the DR, α, and ΔL mean values were added to the simulation.

(D) Evolution of Lb for 500 simulated cells with initially wide distribution of lengths.

(E) Plot showing the distribution of Lb at the three time points indicated by the gray dashed lines in (D). All cells present at the indicated times were considered to build the Lb distributions.

(F) Plots showing the Lb distributions obtained from experiment and simulation (see Table S1 for input parameter values).

(G) Plot showing the dependence in Lb between mother and daughter cells. The data were obtained from a stochastic simulation of the constant extension model using the same number of cells (n = 1,305) as in the experiment shown in Figure 2. Gray dots represent single-cell data, whereas orange dots represent the average of binned data ±SEM.

(H) Degree of inheritance of Lb over one to five generations in simulations. Each line represents the best linear fit to the single-cell data of Lb for an ancestor and its descendant from the first to fifth generation.

(I) Same plot as in (H) except that the data were derived from the *E. coli* LB experiment.

(J) Evolution of the correlation between Lb from ancestors to descendants over generation expected from the model (black) or observed experimentally (red). The correlation was based on linear regressions of single-cell data. The error bars represent the 95% confidence interval around the slope value.

See also Figures S3 and S5.

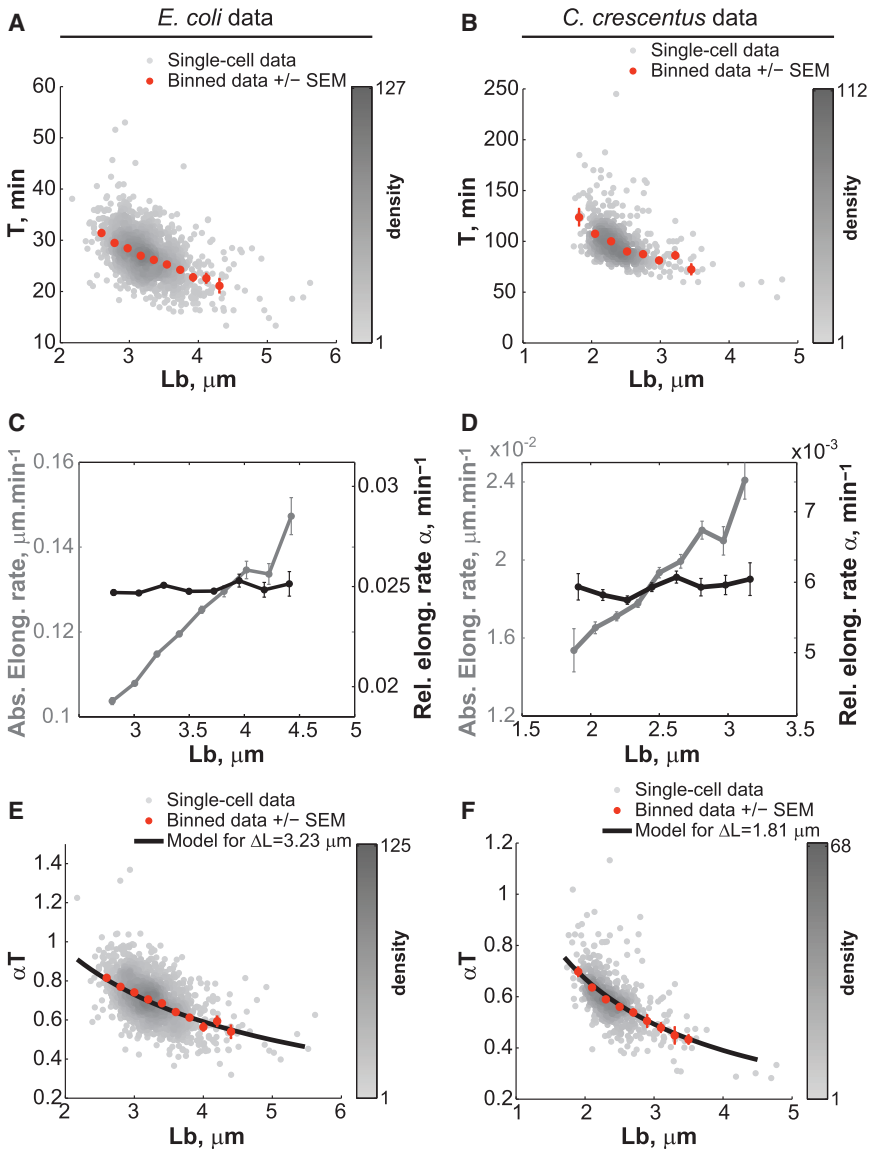

Figure 4. Cells Correct Their Length at Birth by Modulating Their Cell-Cycle Time and Not Their Relative Growth Rate

(A) Dependence of the cell-cycle time T on Lb for *E. coli* grown in LB medium (n = 1,305 cells).

(B) Same as (A) but for *C. crescentus* stalked cells grown in M2G medium (n = 565 cells).

(C) Dependence of the absolute (gray) and relative (black) elongation rate α on Lb for *E. coli*.

(D) Same as (C) but for *C. crescentus*.

(E) Dependence of the normalized cell-cycle time αT on Lb for *E. coli*. The black line represents the expected average αT from the constant extension model, as described by the equation $\alpha T = \ln(1+\Delta L/Lb)$. The black line was drawn using the average ΔL value measured experimentally.

(F) Same as (E) but for *C. crescentus*.

Error bars represent ±SEM.

disruption of glucose transport results in a marked reduction in average ΔL between divisions ($<\Delta L>$ = 1.9 μm for wild-type versus 1.6 and 1.5 μm for Δ*ptsH* and Δ*ptsI*, respectively), without changing the precision of the size homeostasis mechanism ($CV_{\Delta L}$ = 20% for wild-type versus 16 and 18% for Δ*ptsH* and Δ*ptsI*, respectively). These data further support the notion that nutrient availability affects cell size by determining the targeted ΔL that cells will implement at each division cycle.

The Constant Extension Mechanism Has No Memory

The constant extension mechanism is precise, but not perfect, as reflected by the CV of ΔL (Figures S3D and S3E). As such, ΔL values fluctuate around an average value (i.e., the targeted value) from cell to cell and from generation to generation. Importantly, the microfluidic data showed that the constant extension mechanism has no memory, as the ΔL values of mother and daughter cells were not significantly correlated (Figures S5F and S5G, with τ = 0.10 and 0.03 for *E. coli* in M9 an LB media and with τ = 0.06 for *C. crescentus*, respectively). In other words, the accuracy of a cell in implementing the targeted ΔL has no bearing on the precision of its descendants.

Could the Constant Length Extension Be Applied at a Cell-Cycle Event Other Than Division?

So far, we have considered the case of a constant elongation being applied from one division to the next (Figure 6A). But what if the point of control for cell size homeostasis occurs at an earlier cell-cycle event X, and completion of this event X triggers division after a constant amount of time, or timer δt, has elapsed? In this scenario, the constant elongation (referred to as ΔL^* to distinguish it from the elongation ΔL that we actually measured between consecutive divisions) would be applied at this event X, and not at division. For example, this early control event could be the initiation of DNA replication, as theoretically proposed before (Amir, 2014). This is an important consideration, as DNA replication initiation is often assumed to control division. In a scenario in which ΔL^* is applied at cell-cycle event X, the division cycle would be shifted out of phase relative to the constant elongation cycle, and division would follow the completion of a fixed elongation ΔL^* after a timer δt (Figures 6B and 6C). Could this scenario account for the experimental data we obtained?

First, we considered the case in which the timer δt is shorter than the interdivision time T (Figure 6B). This would illustrate the *C. crescentus* situation (T = 100 min) in which DNA replication initiates early in the cell cycle and completes before division (McAdams and Shapiro, 2009). Simulations of the phase-shifted model showed significant discrepancies with the experimental

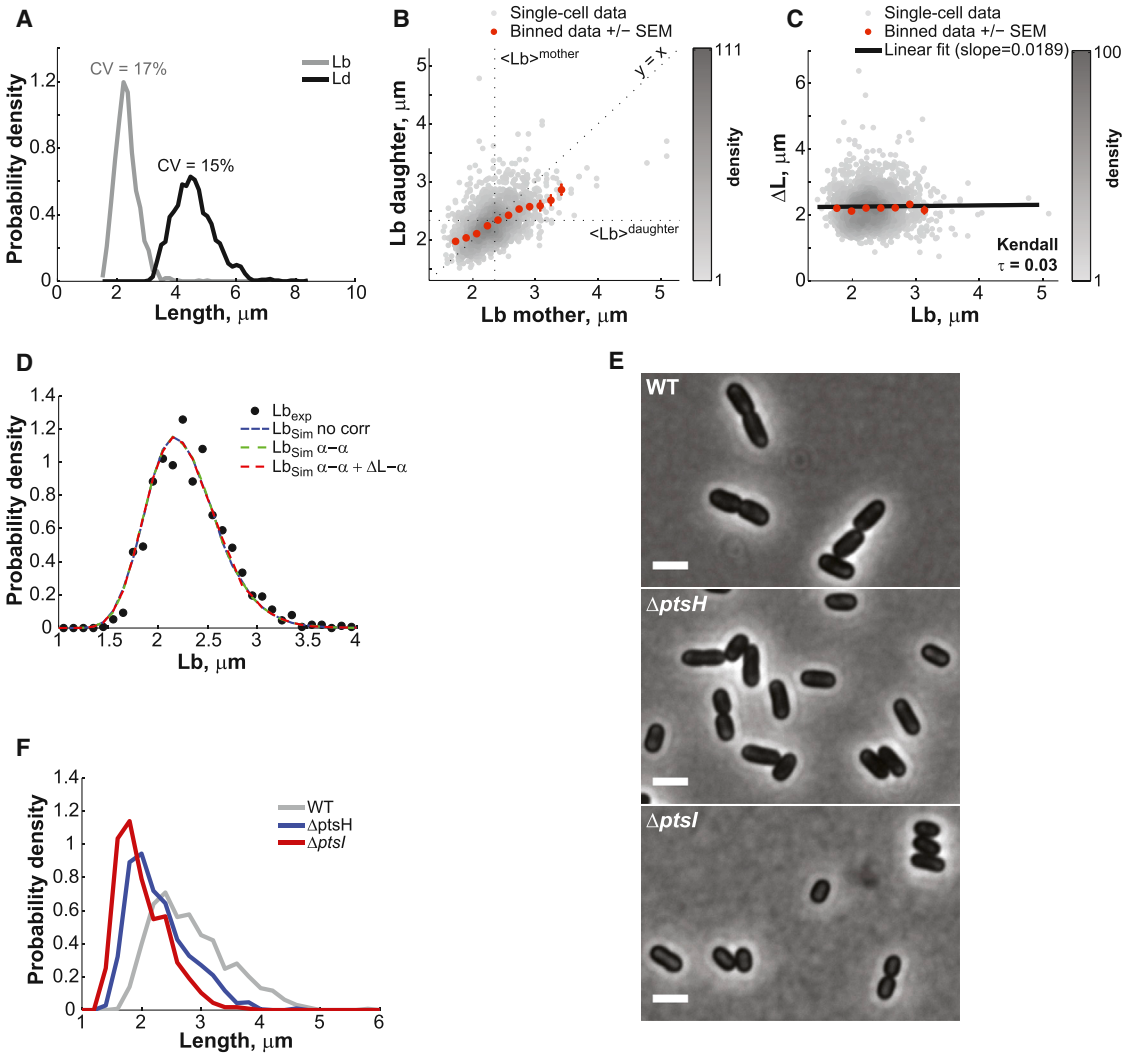

Figure 5. *E. coli* Also Controls Its Length through a Constant Elongation in M9-Supplemented Medium

(A) Distribution of *Lb* and *Ld* of BW25113 cells (n = 1,528) grown in M9-supplemented medium at 32°C in a microfluidic chamber over 6 hr.

(B) Partial inheritance of *Lb* from one generation to the next.

(C) Dependence of ΔL on *Lb*. The black line represents the linear fit to the single-cell data.

(D) Experimental and simulated *Lb* distributions. "No corr," "α-α," and "α-α + ΔL-α" refer to the type of correlations included in the simulations (as described in the Extended Experimental Procedures).

(E) Phase-contrast images of BW25113 wild-type, Δ*pstH*, and Δ*ptsI* grown in M9-supplemented medium in liquid cultures and spotted on 1% agarose pads. Scale bars, 2 μm.

(F) Cell length distributions of wild-type, Δ*pstH*, and Δ*ptsI* populations.

See also Figures S4 and S5.

C. crescentus data for any timer that starts, on average, earlier than at 80% of the division cycle (i.e., for any timer δt > 20 min for T = 100 min). For example, in the phase-shifted model, ΔL (cell length extension between consecutive divisions) and *Lb* show a significant negative correlation (Figure 6D), in contrast to what was observed experimentally (Figure 1G). Other relationships between variables were also inconsistent with the experimental data (Figures S6A–S6C). Therefore, a constant elongation is unlikely to be applied at DNA replication initiation—or at any other early cell-cycle event—to control cell size homeostasis in *C. crescentus*. Whether division was asymmetric (Figures 6D and S6A–S6C) or symmetric (Figures S6D–S6F) did not alter the conclusion.

We also considered the relevant case in which the timer δt would be longer than the interdivision time T (Figure 6C). Previous work has proposed that, in *E. coli*, DNA replication initiation and cell division are separated by a constant timer of about 60 min (Cooper and Helmstetter, 1968), which would exceed the doubling times of 27 and 42 min that we observed for *E. coli* growing in LB and M9 growth media, respectively. To consider these fast-growth cases, we ran simulations of the phase-shifted model with timers longer than the interdivision

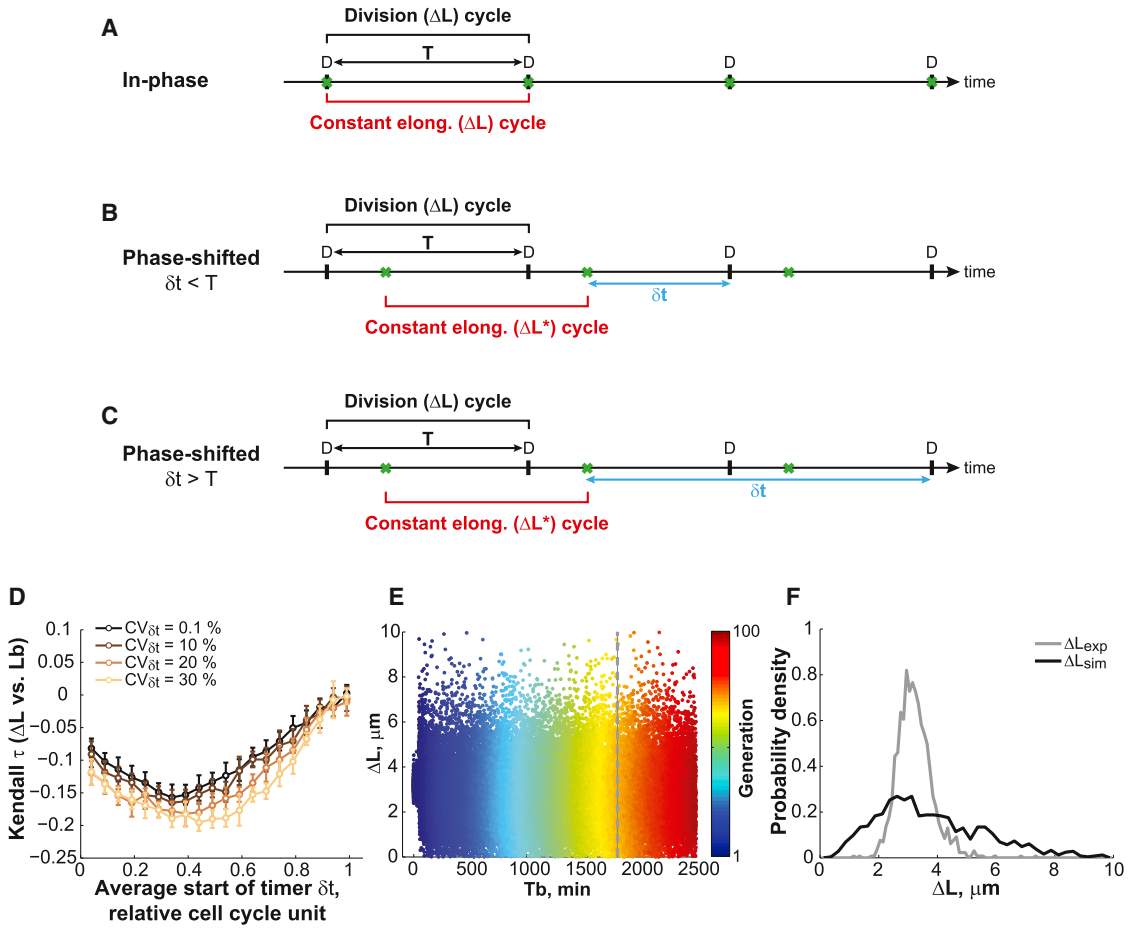

Figure 6. Testing the Phase-Shifted Constant Extension Model

(A) Schematic of the constant extension model in which the division cycle (black bracket) is in phase with the constant elongation cycle (red bracket). The event under cell-cycle control (green crosses) is division D.

(B) Schematic of the "phase-shifted" model with a timer $\delta t < T$. In this model, the elongation increment (ΔL^*) is applied to a cell-cycle event X (green crosses) that is coupled to division by a timer δt shorter than the interdivision time T.

(C) Schematic representation of the "phase-shifted" constant extension model with $\delta t > T$ and with the constraint of a single event X per division cycle (see Extended Experimental Procedures and Table S1).

(D) Simulations of the "phase-shifted" model with a timer $\delta t < T$ (see Extended Experimental Procedures and Table S1). The Kendall correlation coefficient between Lb and ΔL depends on how early in the cell cycle the timer δt starts. Shown is the mean ± SD of ten simulations performed with 1,500 cells for $DR = 0.56$.

(E) Simulations of the "phase-shifted" model with a timer $\delta t > T$. Shown is a scatter plot of ΔL (from birth to division) for 500 simulated cells at each generation.

(F) Same as (E) but plot showing the distribution of ΔL at the time indicated by the dashed line in (E).

See also Figure S6.

times. They resulted in the generation of widely abnormal cell size distributions (Figures S6G and S6H), which arose from the fluctuation in number of event X (e.g., DNA replication initiation) occurring between two divisions. Even when event X was forced to happen exactly once per division cycle (by adding constraining rules to the model, see Extended Experimental Procedures) to reduce the Lb variability, the ΔL values remained aberrantly variable (Figures 6E and 6F). Furthermore, the cell length extension between divisions (ΔL) was correlated between mothers and daughters in the simulated data (Figure S6I); that is, this phase-shifted model with $\delta t > T$ displays memory because the constant elongation ΔL^* overlaps with two consecutive division cycles (Figure 6C). This correlation in ΔL between mothers and daughters is in contradiction with the experimental data (compare Figures S5F and S5G with Figure S6I).

Collectively, these experimental results are inconsistent with the hypothesis that the constant elongation is applied at the initiation of DNA replication or any cell-cycle event that occurs within the first 80% of the interdivision time. This also excludes the formation of the FtsZ cytokinetic ring, implying that this event is unlikely to dictate the timing of cell division. This is in agreement with single-cell observations that FtsZ ring formation and cell constriction are uncorrelated in time (Tsukanov et al., 2011). Our analysis suggests that the cycles of constant elongation and division are in phase or are close to it (Figure 6A), indicating that a late cell-cycle stage is the control point. For instance, a late

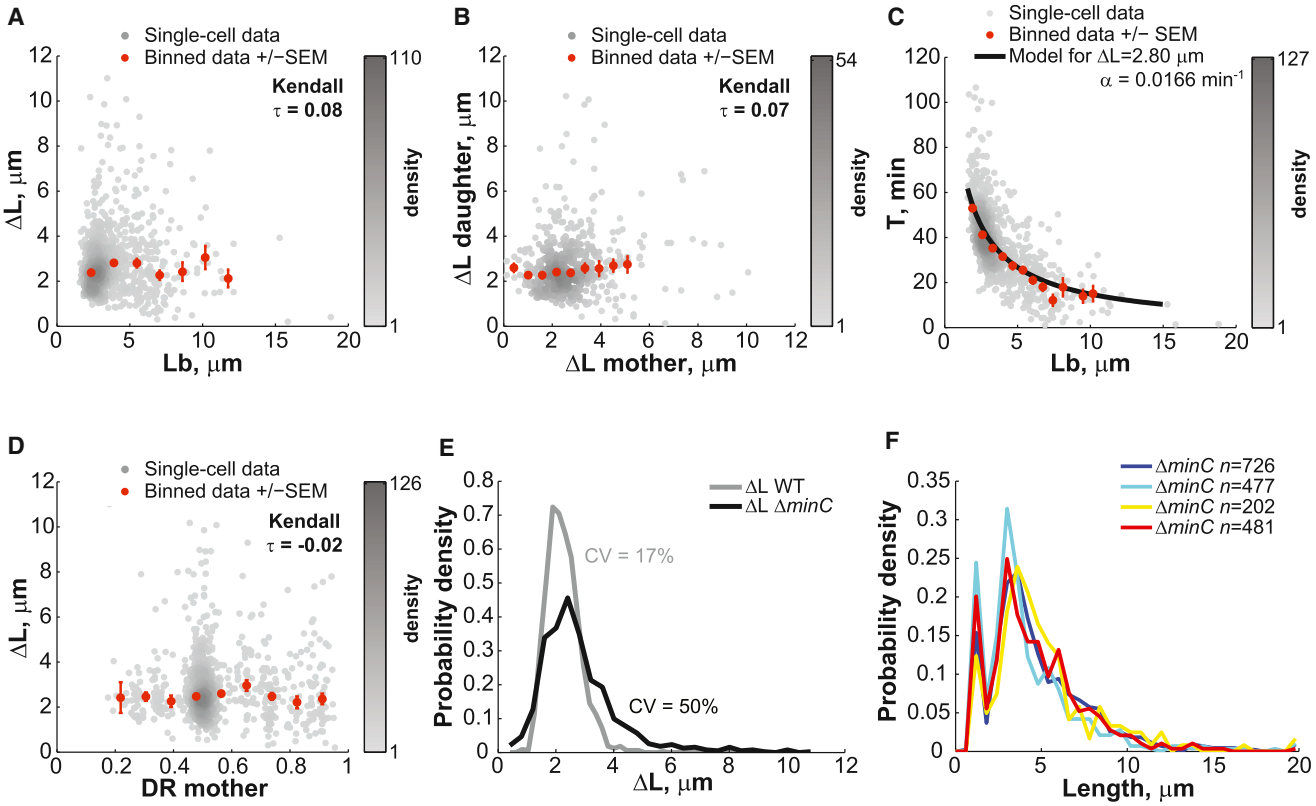

Figure 7. The Constant Extension Mechanism Is Robust with Respect to the Cell Length and Division Site Placement

E. coli BW25113 Δ*minC* cells were grown in microfluidic chambers at 30°C in M9-supplemented medium over 5.5 hr.

(A) Dependence of ΔL on *Lb* (n = 959 cells). Gray dots represent single-cell data, whereas orange dots represent the average of binned data ± SEM.

(B) Degree of inheritance of ΔL over one generation (n = 510 cells).

(C) Dependence of the cell-cycle time *T* on *Lb* (n = 959 cells). The black line represents the expected average αT from the constant elongation model, as described by the equation $T = \ln(1+\Delta L/Lb)/\alpha$. The black line was drawn using the average ΔL and α values measured experimentally.

(D) Dependence of ΔL on *DR*.

(E) Distributions of length extensions for wild-type and Δ*minC* cells.

(F) Cell length distributions of BW25113 Δ*minC* cells grown in separate 2 ml liquid cultures in M9-supplemented medium.

See also Movie S3.

cell-cycle event (e.g., a late step of chromosome segregation potentially sensed by FtsK) may communicate with the cell division machinery to trigger FtsZ ring constriction. Division would then restart a cycle of constant length extension.

The Constant Extension Mechanism Is Robust with Respect to Cell Length and Division Positioning

In the constant extension model, cell size homeostasis is based on a simple governing principle: cells trigger division once they have elongated the targeted ΔL (±noise). Does the simple rule of adding a constant length still apply when cells are aberrantly long or when division is misplaced? To address this question, we carried out microfluidic experiments with the *E. coli* Δ*minC* mutant (Movie S3). Without MinC, the min system that regulates the precision of FtsZ ring placement is defective; as a result, cells divide not only at midcell, but also at polar, DNA-free regions, resulting in the appearance of minicells (Adler et al., 1967). As expected, the large imprecision in division placement in the Δ*minC* mutant leads to very wide distribution of cell lengths at birth (CV of *Lb* = 52%). But despite these aberrations, Δ*minC* cells elongated a constant amount between divisions, regardless of their length at birth (Figure 7A, Kendall τ = 0.08; anucleate minicells were excluded from the analysis, as they do not grow). Even very long cells grew, on average, the same amount as short cells before dividing (Figure 7A). Thus, the constant extension mechanism is insensitive to cell length, as predicted by the model.

Similarly to what was observed for wild-type cells, there was no memory with respect to elongation for Δ*minC* cells, as ΔL between mothers and daughters remained uncorrelated (Figure 7B). Also, as shown in Figure 7C, constant elongation in Δ*minC* cells was achieved by modulating the interdivision time *T* (and not the growth rate, data not shown). The Δ*minC* data showcased the striking agreement between the average cell behavior and the analytical expression of the constant extension model over a wide range of cell lengths (binned data versus black line, Figure 7C).

The Δ*minC* data also demonstrated that cell elongation is independent of where division occurs (Figure 7D). Even when a

division occurred at a pole (producing a minicell), the viable offspring, which inherited all of the genetic material and most of the cytoplasmic and membrane content of the mother, implemented a constant elongation just like cells generated by a normal division. Thus, it is the process of division itself, and not the partitioning of cellular content, that resets the constant extension mechanism.

Another interesting aspect of the Δ*minC* mutant is that it has a moderate chromosome segregation defect (Jaffé et al., 1988) and a skewed distribution of ΔL toward higher values (Figure 7E). We envision two possibilities by which a partial DNA segregation defect can result in tailed ΔL distribution.

DNA segregation may be part of a fail-safe or checkpoint mechanism that is superimposed over the constant extension mechanism. In this scenario, chromosome segregation would normally occur within the time needed to grow the appropriate ΔL and divide, having no impact on the constant extension mechanism. However, if DNA segregation becomes abnormal and does not complete within this time period, a fail-safe mechanism would override the constant extension mechanism by delaying division. Such override may occur through so-called "nucleoid occlusion" (Wu and Errington, 2012), which is known to interfere with FtsZ ring assembly in *E. coli*. A delay in division would result in higher ΔL values than expected. Note that any fail-safe mechanism that blocks a step required for division as a response to a defect would override the constant extension mechanism until the defect is resolved. A good example is the SOS response to DNA damage that blocks division until DNA repair is completed (Huisman and D'Ari, 1981).

Alternatively, DNA segregation may be an inherent part of the constant extension mechanism, with the nucleoid acting as a molecular ruler. For example, cell extension may be involved in nucleoid separation, which in turn may trigger cell constriction, perhaps by relieving some form of DNA occlusion. A defect in DNA segregation would then delay division, leading to higher ΔL values. Future studies will be required to distinguish between these two possibilities.

Defining Features of the Constant Extension Mechanism

A constant extension mechanism strongly departs conceptually from the deeply rooted critical size paradigm. In all sizer-based models, cells "sense" how big they are, whereas in the constant extension model, cells are blind to their size and instead "sense" how much they have grown. It is important to note that, although we are measuring cell length, cells may be "measuring" a difference in any cell size parameter; it could be a difference in cell length, but it could also be a difference in cell mass, surface area, or volume, as cell width does not change during the cell cycle.

Our findings suggest that cells follow the simple rule of triggering division when they have elongated the targeted ΔL. This is sufficient to provide a cell size homeostasis mechanism. We have identified several defining features of this cell size homeostasis mechanism. (1) Cell size deviations are abated exponentially over generations (Figure 3J). (2) The constant extension mechanism does not need to be precise (Figure 3), with experimental $CV_{\Delta L}$ of 19%–26%. A greater variability in ΔL among cells would increase the variability in cell length at birth but would not affect the average cell length of the population or the homeostatic capability of the mechanism. (3) The constant extension mechanism provides cell size homeostasis that is robust with respect to cell length and division placement. Our Δ*minC* data explicitly demonstrate the robustness of the mechanism: despite aberrant cell lengths at birth, wide imprecision of division placement, and large variation in cell elongation, Δ*minC* cells maintain a stable cell size distribution over time (data not shown) and from culture to culture (Figure 7F). (4) Any division, including nonproductive ones that create minicells, resets the constant extension mechanism. (5) Any imprecision in size extension at one generation has no impact on the precision at the next generation (Figures S5F and S5G). These defining features provide a strong foundation for future molecular studies and will have to be accounted for by any molecular models of the constant extension mechanism.

Several lines of evidence suggest that a constant cell extension might be an ancient and broadly applicable means of achieving cell size homeostasis. *E. coli* and *C. crescentus* are evolutionary distant, having diverged more than one billion year ago. Their divisions (symmetric versus asymmetric) are distinct. *E. coli* changes its length according to nutrient availability, whereas *C. crescentus* does not. *E. coli* can undergo overlapping rounds of DNA replication, whereas this has never been observed for *C. crescentus*. Despite these profound differences in growth, division, and replication cycle, a similar cell size control operates, suggesting that this size homeostatic model is applicable to a wide variety of bacterial species under different growth conditions.

EXPERIMENTAL PROCEDURES

Strains and Media

C. crescentus CB15N (Evinger and Agabian, 1977) and *Escherichia coli* K12 strain BW25113 (Datsenko and Wanner, 2000) were used for the experiments unless indicated. *E. coli* BW25113 and Δ*minC*, Δ*ptsH*, and Δ*ptsI* derivatives were obtained from the Yale *E. coli* Genetic stock center. *C. crescentus* CB15N was grown either in PYE medium (2 g/l bacto-peptone, 1 g/l yeast extract, 1 mM $MgSO_4$, 0.5 mM $CaCl_2$) or M2G medium (0.87 g/l Na_2HPO_4, 0.54 g/l KH_2PO_4, 0.50 g/l NH_4Cl, 0.2% (w/v) glucose, 0.5 mM $MgSO_4$, 0.5 mM $CaCl_2$, 0.01 mM $FeSO_4$). *E. coli* BW25113 was grown in LB medium (10 g/l NaCL, 5 g/l yeast extract, 10 g/l tryptone), or M9-supplemented medium (6 g/l $Na_2HPO_4 \cdot 7H_2O$, 3 g/l KH_2PO_4, 0.5 g/l NaCl, 1 g NH_4Cl, 2 mM $MgSO_4$, 1 μg/l thiamine supplemented with 0.1% casamino acids and 0.2% glucose).

Microscopy

C. crescentus cells were grown up to exponential phase ($OD_{660nm} < 0.3$) and were spotted on 0.3% agarose pads containing M2G medium unless specified otherwise. Microscopy was performed on an Eclipse 80i microscope (Nikon) equipped with a phase-contrast objective Plan Apochromat 100×/1.40 NA (Nikon), an Orca-II-ER (Hamamatsu Photonics), and an Andor iXon DU-897E camera (Andor Technology) with 2× optivar. Images were acquired every 2.5 min using MetaMorph software (Molecular Devices).

For still images of *E. coli* strains, cells were grown at 30°C up to exponential phase ($OD_{600nm} < 0.3$) and were spotted on 1% agarose pads. For microfluidic experiments, *E. coli* cells were loaded and grown for at least five generations in the microfluidic device prior to imaging. Microscopy was performed on an Eclipse Ti-E microscope (Nikon) equipped with Perfect Focus System (Nikon) and an Orca-R2 camera (Hamamatsu Photonics) and a phase-contrast objective Plan Apochromat 100x/1.45 NA (Nikon). Time-lapse images were acquired every 5 s using NIS-Element Ar software (Nikon Instruments).

Stochastic Simulations

Numerical simulations of evolving cell populations were done in MATLAB using probability density distributions matching experimentally measured distributions (Figure S7 and Table S1) as described in the Extended Experimental Procedures.

SUPPLEMENTAL INFORMATION

Supplemental Information includes Extended Results, Extended Experimental Procedures, seven figures, one table, and three movies and can be found with this article at http://dx.doi.org/10.1016/j.cell.2014.11.022.

AUTHOR CONTRIBUTIONS

M.C., I.V.S., and S.K. contributed equally to this work. S.K., M.C., and C.J.-W. conceived the project, designed the experiments, and analyzed the data. M.C., S.K., and S.E.E. performed the experiments. I.V.S. and B.B. developed mathematical models, and I.V.S., B.B., and M.C. performed simulations. A.P. assisted in data analysis. M.C., I.V.S., and C.J.-W. wrote the paper. All authors commented on and approved the paper.

ACKNOWLEDGMENTS

We would like to thank Dr. Johan Elf for sharing the design of his microfluidic device, Matts Walden and Jason Hocking for help setting up the microfluidic system in our laboratory, and the Yale *E. coli* genetic stock center for the *E. coli* BW25113 derived strains. This work was, in part, supported by the National Institute of Health (R01 GM065835 to C.J.-W.). S.K. and S.E.E. were, in part, supported by the Astellas Foundation for Research on Metabolic Disorders and a predoctoral training grant of the National Institute of Health (5 T32 GM 7223-39), respectively. We are also grateful to the staffs of the Yale University Faculty of Arts and Sciences High Performance Computing Center for support and to the members of the Jacobs-Wagner laboratory for fruitful discussions and for critical reading of this manuscript. C.J.-W. is an investigator of the Howard Hughes Medical Institute.

Received: August 13, 2014
Revised: October 20, 2014
Accepted: November 13, 2014
Published: December 4, 2014

REFERENCES

Adler, H.I., Fisher, W.D., Cohen, A., and Hardigree, A.A. (1967). Miniature *escherichia coli* cells deficient in DNA. Proc. Natl. Acad. Sci. USA *57*, 321–326.

Akerlund, T., Nordström, K., and Bernander, R. (1995). Analysis of cell size and DNA content in exponentially growing and stationary-phase batch cultures of Escherichia coli. J. Bacteriol. *177*, 6791–6797.

Amir, A. (2014). Cell Size Regulation in Bacteria. Phys. Rev. Lett. *112*, 208102.

Bates, D., and Kleckner, N. (2005). Chromosome and replisome dynamics in E. coli: loss of sister cohesion triggers global chromosome movement and mediates chromosome segregation. Cell *121*, 899–911.

Boye, E., and Nordström, K. (2003). Coupling the cell cycle to cell growth. EMBO Rep. *4*, 757–760.

Cooper, S. (1991). Bacterial Growth and Division: Biochemistry and Regulation of Prokaryotic and Eukaryotic Division Cycles, First Edition, *Volume 1* (San Diego, CA: Academic Press).

Cooper, S., and Helmstetter, C.E. (1968). Chromosome replication and the division cycle of Escherichia coli B/r. J. Mol. Biol. *31*, 519–540.

Datsenko, K.A., and Wanner, B.L. (2000). One-step inactivation of chromosomal genes in Escherichia coli K-12 using PCR products. Proc. Natl. Acad. Sci. USA *97*, 6640–6645.

Di Talia, S., Skotheim, J.M., Bean, J.M., Siggia, E.D., and Cross, F.R. (2007). The effects of molecular noise and size control on variability in the budding yeast cell cycle. Nature *448*, 947–951.

Donachie, W.D. (1968). Relationship between cell size and time of initiation of DNA replication. Nature *219*, 1077–1079.

Evinger, M., and Agabian, N. (1977). Envelope-associated nucleoid from Caulobacter crescentus stalked and swarmer cells. J. Bacteriol. *132*, 294–301.

Evinger, M., and Agabian, N. (1979). Caulobacter crescentus nucleoid: analysis of sedimentation behavior and protein composition during the cell cycle. Proc. Natl. Acad. Sci. USA *76*, 175–178.

Fantes, P.A. (1977). Control of cell size and cycle time in Schizosaccharomyces pombe. J. Cell Sci. *24*, 51–67.

Fantes, P.A., and Nurse, P. (1981). Division timing: controls, models and mechanisms. In The cell cycle, P.C.L. John, ed. (New York City: Cambridge University Press), pp. 11–34.

Harris, L.K., Dye, N.A., and Theriot, J.A. (2014). A Caulobacter MreB mutant with irregular cell shape exhibits compensatory widening to maintain a preferred surface area to volume ratio. Mol. Microbiol. http://dx.doi.org/10.1111/mmi.12811.

Hosoda, K., Matsuura, T., Suzuki, H., and Yomo, T. (2011). Origin of lognormal-like distributions with a common width in a growth and division process. Phys. Rev. E. Stat. Nonlin. Soft Matter Phys. *83*, 031118.

Huisman, O., and D'Ari, R. (1981). An inducible DNA replication-cell division coupling mechanism in E. coli. Nature *290*, 797–799.

Jaffé, A., D'Ari, R., and Hiraga, S. (1988). Minicell-forming mutants of Escherichia coli: production of minicells and anucleate rods. J. Bacteriol. *170*, 3094–3101.

Johnston, G.C., Pringle, J.R., and Hartwell, L.H. (1977). Coordination of growth with cell division in the yeast Saccharomyces cerevisiae. Exp. Cell Res. *105*, 79–98.

Koch, A.L., and Schaechter, M. (1962). A model for statistics of the cell division process. J. Gen. Microbiol. *29*, 435–454.

Koppes, L.J., Meyer, M., Oonk, H.B., de Jong, M.A., and Nanninga, N. (1980). Correlation between size and age at different events in the cell division cycle of Escherichia coli. J. Bacteriol. *143*, 1241–1252.

Lord, P.G., and Wheals, A.E. (1981). Variability in individual cell cycles of Saccharomyces cerevisiae. J. Cell Sci. *50*, 361–376.

McAdams, H.H., and Shapiro, L. (2009). System-level design of bacterial cell cycle control. FEBS Lett. *583*, 3984–3991.

Osella, M., Nugent, E., and Cosentino Lagomarsino, M. (2014). Concerted control of Escherichia coli cell division. Proc. Natl. Acad. Sci. USA *111*, 3431–3435.

Robert, L., Hoffmann, M., Krell, N., Aymerich, S., Robert, J., and Doumic, M. (2014). Division in Escherichia coli is triggered by a size-sensing rather than a timing mechanism. BMC Biol. *12*, 17.

Santi, I., Dhar, N., Bousbaine, D., Wakamoto, Y., and McKinney, J.D. (2013). Single-cell dynamics of the chromosome replication and cell division cycles in mycobacteria. Nat. Commun. *4*, 2470.

Schaechter, M., Maaloe, O., and Kjeldgaard, N.O. (1958). Dependency on medium and temperature of cell size and chemical composition during balanced grown of Salmonella typhimurium. J. Gen. Microbiol. *19*, 592–606.

Schaechter, M., Williamson, J.P., Hood, J.R., Jr., and Koch, A.L. (1962). Growth, cell and nuclear divisions in some bacteria. J. Gen. Microbiol. *29*, 421–434.

Siegal-Gaskins, D., and Crosson, S. (2008). Tightly regulated and heritable division control in single bacterial cells. Biophys. J. *95*, 2063–2072.

Sliusarenko, O., Heinritz, J., Emonet, T., and Jacobs-Wagner, C. (2011). High-throughput, subpixel precision analysis of bacterial morphogenesis and intracellular spatio-temporal dynamics. Mol. Microbiol. *80*, 612–627.

Sveiczer, A., Novak, B., and Mitchison, J.M. (1996). The size control of fission yeast revisited. J. Cell Sci. *109*, 2947–2957.

Terrana, B., and Newton, A. (1975). Pattern of unequal cell division and development in Caulobacter crescentus. Dev. Biol. *44*, 380–385.

Tsukanov, R., Reshes, G., Carmon, G., Fischer-Friedrich, E., Gov, N.S., Fishov, I., and Feingold, M. (2011). Timing of Z-ring localization in Escherichia coli. Phys. Biol. *8*, 066003.

Turner, J.J., Ewald, J.C., and Skotheim, J.M. (2012). Cell size control in yeast. Curr. Biol. *22*, R350–R359.

Ullman, G., Wallden, M., Marklund, E.G., Mahmutovic, A., Razinkov, I., and Elf, J. (2013). High-throughput gene expression analysis at the level of single proteins using a microfluidic turbidostat and automated cell tracking. Philos. Trans. R. Soc. Lond. B. Biol. Sci. *368*, 20120025.

Voorn, W.J., and Koppes, L.J. (1998). Skew or third moment of bacterial generation times. Arch. Microbiol. *169*, 43–51.

Wakamoto, Y., Ramsden, J., and Yasuda, K. (2005). Single-cell growth and division dynamics showing epigenetic correlations. Analyst (Lond.) *130*, 311–317.

Wang, P., Robert, L., Pelletier, J., Dang, W.L., Taddei, F., Wright, A., and Jun, S. (2010). Robust growth of Escherichia coli. Curr. Biol. *20*, 1099–1103.

Wold, S., Skarstad, K., Steen, H.B., Stokke, T., and Boye, E. (1994). The initiation mass for DNA replication in Escherichia coli K-12 is dependent on growth rate. EMBO J. *13*, 2097–2102.

Wu, L.J., and Errington, J. (2012). Nucleoid occlusion and bacterial cell division. Nat. Rev. Microbiol. *10*, 8–12.

EXTENDED RESULTS

Correlations in Growth Rates or Growth Rate/Cell Length Increment Do Not Play a Role in Cell Size Regulation

Interestingly, we observed correlations in the M9 data that were absent in the LB data set. In the M9 medium, the relative growth rates of mother and daughter cells were positively correlated, with a Kendall correlation coefficient $\tau = 0.30$ (Figure S5A) versus $\tau = 0.09$ in LB medium (Figure S5C). A positive correlation was also measured between the elongation ΔL and the relative growth rate α in M9 medium with $\tau = 0.40$ (Figure S5B) versus $\tau = -0.01$ in LB medium (Figure S5D). The reason for these differences in correlation between the two medium conditions is not clear. But importantly, these correlations appear to have no effect on the constant extension model as simulations precisely predicted the experimental distribution of length at birth *Lb*, regardless whether these correlations were considered or not (Figure 5D and Figure S5E). In the *C. crescentus* data set, there was almost no correlation between α and ΔL (Kendall $\tau = 0.12$, Figure S5J). However, the growth rate of the daughter cells was positively correlated with the growth rate of their mothers (Kendall $\tau = 0.34$, Figure S5K). But again, this correlation had no effect on cell size regulation (data not shown).

EXTENDED EXPERIMENTAL PROCEDURES

Microfluidic Devices

Microfluidic devices were fabricated by molding polydimethylsiloxane (PDMS Slygard 184, Dow Corning) to the master molds (Ullman et al., 2013). The master molds were fabricated using standard UV-soft lithography techniques. Two layers of epoxy (Su-8 s, MicroChem) patterned by negative photo-transparency chrome masks were sequentially cross-linked on silicon wafers by UV irradiation. The thickness of the first layer determines the depth of the growth chambers while the thickness of the second one determines the depth of the flow channels. The layer for growth chambers (~0.95-μm or ~1.20-μm thick) was deposited first using SU-8 2000.5 or a mixture of SU8 2000.5 and SU8 2005 at a ratio of 1:4 and processed according to manufacturer's manual. On top of the first layer, the second layer for channels (~5-μm thick) was deposited using SU-8 2005.

A cast of the mold was made of PDMS by pouring a mixture of catalyst and resin at a 1:15 ratio. The cast was degassed for 1 hr and cured in an 80°C oven for 2 hr. One master cast contained 12 identical chip structures, which could be excised and used individually. After the PDMS was peeled off the mold, inlet and outlet holes (diameter ≈0.5 mm) were punctured.

The cast was bonded to a #1 coverslip (22x60 mm, Thermo-Scientific) after oxygen/UV plasma treatment (PDC-32G, Harrick Plasma, NY) for 1 min at an oxygen pressure of ~0.75 bar. The bond was stabilized by incubating at 80°C for 10 min.

The flow of media in the device was controlled by adjusting the relative elevation of the different reservoirs.

Image Processing

Cell outlines were detected using a modified version of the MicrobeTracker software (Sliusarenko et al., 2011). All data processing was then performed using MATLAB (MathWorks). For the *C. crescentus* data, the polarity of cell outlines was set by visual detection of the stalk. All tracked cells were visually inspected. For microfluidic experiments, we used an in-house, Linux-compatible version of MicrobeTracker (to be published elsewhere) so as to manage the size of the data sets. Post-image analysis of microfluidic experiments was performed in MATLAB.

Data Processing and Analysis

For the *E. coli* microfluidic data set, a conservative automatic pruning of data was applied to exclude any cell that (1) was tracked for less than 4 min, (2) was without an ancestor, (3) did not have exactly two daughter cells, (4) had two daughter cells of widely different sizes (the longest being over 80% of the mother's length), (5) approached the edge of the growth chamber by less than 640 nm (10 pixels) during the last 50 frames of their cell cycle (~4 min), and (6) decreased in length over the second half of the cell cycle. The data for all the other cells were collected and organized into a precleaned data set. In the case of the *minC* deletion mutant, the lower limit for the interdivision time was omitted, as some cells display a true division cycle shorter than 4 min.

For all experiments, the quality of the cell outlines was verified by visual inspection. For all selected cells, eight parameters (*Lb*, *Ld*, *Tb*, *Td*, *T*, α, ΔL, *DR*) were quantified. For *C. crescentus* time lapses, we defined the time of the division *Td* as the frame preceding the one where the swarmer progeny swims away (i.e., following physical separation of the two daughter cells). For *E. coli* time lapses, cell division was automatically detected based on the level of constriction of the cells (Sliusarenko et al., 2011). The time of division (*Td*) was defined as the frame preceding the division. Since cell birth happens at cell division, the birth time (*Tb*) of a cell was defined as a time of the cell division of its mother cell (i.e., one frame before the newborn cell was detected for the first time) for both *E. coli* and *C. crescentus*. The cell cycle time *T* was the elapsed time between the times at birth and division: $T = Td - Tb$. Length at division *Ld* and length at birth *Lb* were measured at times *Td* and *Tb*, respectively. *Ld* was obtained from the cell outline, while *Lb* was calculated as the length of the mother cell multiplied by its division ratio. Division ratio *DR* was determined from the phase contrast profile of the mother cell at *Td* as previously described (Sliusarenko et al., 2011). ΔL was calculated as $\Delta L = Ld - Lb$. The elongation rate α was obtained from the single-cell growth curves by fitting the logarithm of the length with the linear mode: $log(L(t)) = \alpha t + log(Lb)$, where $L(t)$ is the length of a cell at time t and *Lb* the cell at birth. In the case of the *E. coli* microfluidic experiments, the cell length is overestimated by the cell outline at the beginning of the cell cycle, as a result of the daughter

cells still touching each other. To avoid any systematic bias in the result of the fit, only the second half of the growth curve was used for the fitting. For the *C. crescentus* soft-agar data set, the parameters *Lb*, *Ld*, *Tb*, *Td*, *T*, α, ΔL *and DR* were defined as described above, except that for *DR*, the relative position of the division site was calculated from the stalked pole and that *Lb* was determined at the first frame after division of the mother cell.

The average cell length at birth of *C. crescentus* swarmer cells identified during the experiments on 0.3% agarose pads, as defined by the length of the mother cell at the frame at division multiplied by the division ratio, was shorter than the average cell length at birth of the swarmer cells that we tracked for a full cell cycle on the 0.3% agarose pads. This result suggests that longer swarmer cells have a higher probability of immobilizing on the soft agar pads.

The analysis of the publicly available *E. coli* data set from the "mother machine" microfluidic experiments (Wang et al., 2010) was focused on the cell number 0 of each channel (first daughter) so as to avoid any size bias against long cells. We selected all cells that met the following requirements: (1) *Lb* was the smallest cell length among the lengths measured from 5 frames (or 5 min) before and after birth. (2) The cell cycle time *T* was longer than 3 frames (3 min). (3) Cell length was smaller than 20 μm at any time. (4) The sum of the squared error of the growth curve fitting divided by the degree of freedom was smaller than 0.001.

Constant Extension Model

In the absence of knowledge about whether the cells 'sense' a difference in length, surface area or volume, we used cell length as a catch-all descriptor to define cell size because i) cell width does not change during the cell cycle and ii) determination of cell surface area or volume is not as accurate as they require some assumption about the cell geometry. Nonetheless, the model described below is equally applicable to cell length (*L*), mass (*M*), surface area (*SA*) and volume (*V*). *L* would simply be replaced by *M*, *SA* or *V* in the equations.

If a cell always elongates by the exact same amount ΔL during cell cycle (i.e., there is no fluctuations in ΔL):

$$Lb_{i+1} = (Lb_i + \Delta L)DR, \tag{1}$$

where *i* denotes the generation, *Lb* is the cell length at birth, and *DR* is the division ratio. Then, cell length changes from generation to generation as

$$Lb_{i+1} = (Lb_i + \Delta L)DR = Lb_0 DR^{i+1} + \Delta L \frac{1 - DR^{i+1}}{1 - DR} DR \tag{2}$$

For symmetric divisions (*DR* = 1/2), the equation becomes

$$Lb_{i+1} = Lb_0 2^{-(i+1)} + \Delta L\left(1 - 2^{-(i+1)}\right) \tag{3}$$

Equations 2 and 3 show that if the cell length at birth deviates from the "target" size (i.e., the mean of the population at the given conditions) at some generation (with its length noted as Lb_0), then the cell length at birth will converge exponentially over generations to a steady-state value of ΔL *DR* / (1 - *DR*), no matter how large the original deviation was. Equation 2 and 3 also show that, if ΔL values fluctuate stochastically around some mean value and do not correlate with *Lb*, then the expected correlation of cell sizes at birth in subsequent generations decays as $2^{-(i+1)}$.

For cells growing exponentially, elongation is linked to the size at birth as

$$\Delta L = Lb\ \left(e^{\alpha T} - 1\right), \tag{4}$$

where α is the relative growth rate and *T* is the duration of the cell cycle. We define a 'normalized cell cycle time' $\alpha\ T$ as:

$$\alpha T = ln\left(1 + \frac{\Delta L}{Lb}\right). \tag{5}$$

Calculations of the Mean and Variance of Cell Lengths at Birth

In real cells, both ΔL and *DR* fluctuate around their mean values, leading to fluctuations in *Lb*. For simplicity of exposition, let $P_1(Lb)$, $P_2(\Delta L)$, and $P_3(DR)$ denote the steady-state probability density functions of *Lb*, ΔL, and *DR*, respectively. We note that the following calculation can be made rigorous, with the same result, in the case when *Lb*, ΔL, and *DR*, have no density functions. We write the probability of observing a cell born with a length *x*, elongated by ΔL and divided with ratio *DR* as:

$$P_1(x)\mathrm{d}x\ P_2(\Delta L)\mathrm{d}\Delta L\ P_3(DR)\mathrm{d}DR. \tag{6}$$

We consider the case where $P_1(Lb)$ and $P_2(\Delta L)$ are independent of each other and are also independent of $P_3(DR)$, as shown experimentally (Figures 1G and H, 2F and 5C and Figures S2, S5H, S5I, and S5L and S7A, S7B).

At steady state, keeping only one offspring (as in the *C. crescentus* experiment, where we tracked only the stalked cells) the probability that a cell is born at length *Lb* is the integral of (6) over all combinations of lengths, increment sizes, and division ratios (*x*, ΔL, and *DR*) satisfying Equation 1:

$$P_1(Lb) = \int P_1(x)\, P_2(\Delta L)\, P_3(DR)\delta(Lb\text{-}(x+\Delta L)DR)\mathrm{d}x\, \mathrm{d}\Delta L\, \mathrm{d}DR, \tag{7}$$

where δ denotes Dirac delta function. Equation 7 is an integral equation that defines $P_1(Lb)$ for a given $P_2(\Delta L)$ and $P_3(DR)$. To calculate the mean of $P_1(Lb)$, we integrate Equation 7:

$$\langle Lb\rangle = \int Lb\, P_1(x)\, P_2(\Delta L)\, P_3(DR)\delta(Lb\text{-}(x+\Delta L)DR)\mathrm{d}x\, \mathrm{d}\Delta L\, \mathrm{d}DR\, \mathrm{d}LB. \tag{8}$$

Taking into account the independence of P_1, P_2, and P_3 and that $\int x\, P_1(x)\, \mathrm{d}x = < Lb >$, $\int \Delta L\, P_2(\Delta L)\, \mathrm{d}\Delta\mathrm{L} = < \Delta L >$ and $\int DR\, P_2(DR)\, \mathrm{d}DR = < DR >$, Equation 8 leads to

$$\langle Lb\rangle = \langle \Delta L\rangle \frac{\langle DR\rangle}{1-\langle DR\rangle}. \tag{9}$$

For symmetric divisions ($DR = 1/2$), the equation becomes

$$\langle Lb\rangle = \langle \Delta L\rangle \tag{10}$$

Similarly, we can calculate the second moment $< Lb^2 > = \int Lb^2\, P_1\, (Lb)\, \mathrm{d}Lb$ from Equation 7 as

$$\langle Lb^2\rangle = \langle \Delta L^2\rangle \frac{\langle DR^2\rangle}{1-\langle DR^2\rangle}\left(1+2\frac{\langle \Delta L\rangle\langle Lb\rangle}{\langle L^2\rangle}\right). \tag{11}$$

For symmetric divisions ($DR = 1/2$), the equation becomes

$$\langle Lb^2\rangle = \langle \Delta L^2\rangle \frac{\langle DR^2\rangle}{1-\langle DR^2\rangle}\left(1+2\frac{\langle \Delta L\rangle^2}{\langle \Delta L^2\rangle}\right). \tag{12}$$

The variance is calculated from Equations (9) and (11) as

$$\mathrm{var}(Lb) = \langle Lb^2\rangle\text{-}\langle Lb\rangle^2. \tag{13}$$

Equations 9 and 11 allow the calculation of the mean and variance of *Lb* without any assumptions on the particular shape of *DR* and ΔL distributions. This approach can also be used to calculate moments of higher orders.

Equations (9), (11) and (13) lead to the following expression for the coefficient of variation of *Lb* (CV_{Lb}):

$$CV_{Lb}^2 = \frac{\left(CV_{DR}^2+1\right)(1-DR_0)^2}{1-\left(CV_{DR}^2+1\right)DR_0^2}\left(CV_{\Delta L}^2+1+2\frac{DR_0}{1-DR_0^2}\right)-1, \tag{14}$$

where DR_0 denotes the mean *DR* value.

For symmetric divisions ($DR = 1/2$),

$$CV_{Lb}^2 = \frac{CV_{DR}^2+1}{3-CV_{DR}^2}\left(CV_{\Delta L}^2+3\right)-1. \tag{15}$$

Note that CV_{Lb} explicitly depends on both $CV_{\Delta L}$ and CV_{DR}, but does not depend on the mean ΔL value and only has a weak dependence on the mean *DR* value.

Estimation of the Mean and CV of ΔL from Still Images

First, we estimated the distributions of *Lb* from length and *DR* measurements of deeply constricted cells from still images. Second, we calculated the mean and CV of ΔL for each strain using the constant extension model (Equations 10 and 15).

Stochastic Simulations

Constant Extension Model

Numerical stochastic simulations of evolving cell populations were done in MATLAB using custom written scripts and built-in random number generators (Mersenne Twister with the "shuffled" option for seeding); note that the choice of different seedings and/or

generators did not change population behavior. Briefly, a given number of cells (n_0) were initialized with a chosen distribution of lengths, and with the same (i.e., $\delta t = 0$, perfectly synchronized cells) or distributed (unsynchronized cells) relative cell cycle times ($\delta t = t / T_d$). Probability density distributions were chosen to match experimentally measured distributions when possible, with means and variances corresponding to values obtained in experiments. In particular, in order to recapitulate the experimental distributions, the division ratio *DR* was always drawn independently of other stochastic variables from a normal distribution (Figure 1C and Figure S7C); the growth rate, α, was drawn from a normal distribution (Figure S7D); and, for the simulations where the constant increment dictates the cell division event, the cell length elongation ΔL was drawn from a log-normal distribution (Figure S7E). Values used in the simulations are summarized in Table S1. In simulations where growth rates were correlated between mother and daughter cells (as observed in M9 supplemented medium experiments, Figure S5A), the mean ($<\alpha_D>$) and the standard deviation (σ_D) values of the α probability distribution were dependent on the mother cell growth rate α_M: $<\alpha_D> = \alpha_0 + c(\alpha_M - \alpha_0)$, $\sigma_D = \sigma_0(1 - c^2)$, where α_0 and σ_0 are the mean and standard deviation of the growth rate distribution, and c is a correlation coefficient. To investigate the role of the correlations between ΔL and α, we generated correlated (ΔL,α) pairs using Gaussian copulas with marginal lognormal and normal distribution for ΔL and α, respectively.

For each cell, the division time was calculated from ΔL and α values as $\ln(1+\Delta L/Lb)/\alpha$. At division, the cell was split into two daughter cells according to *DR*, and in case of asymmetric divisions (as for *C. crescentus*), the cells were labeled "swarmer" or "stalked," respectively. This process was repeated iteratively for a given number of generations. We modeled both continuously expanding (with the number of cells in a population growing exponentially, as in batch cultures) and steady-state (with a near constant number of cells, as in microfluidic experiments) cell populations. In the steady-state case, at each generation, if the number of cells exceeded the allowed maximum n_{max}, the n_{max} of cells was randomly chosen from the current population and the other cells were discarded. Note that this procedure kept a constant amount of cells at any generation while the amount of cells in the population at any given time fluctuates around n_{max} (due to overlaps of generations).

Phase-Shifted Model

For simulations of the model in which a constant elongation increment ΔL^* is applied between consecutive "control" cell cycle event X (e.g., DNA replication initiation) instead of between divisions, the increment ΔL^* was drawn from a log-normal distribution similar to the model described above, as, to our knowledge, there are no experimental measurements of this distribution. The delay time or timer δt between the control cell cycle event X and the cell division it triggers was drawn from a normal distribution, with varying CV. We generated values of *DR* and α for each cell, as described above. For every virtual cell, each control event (at time T_c and cell length L_c) licensed a cell division to happen at time $T_c+\delta t$. Each control event also cued another control event to happen after the cell has grown ΔL^*. In simulations where the number of control events was not artificially restricted, any-non-negative integer number of control events per cycle was possible. If a division happened before the cell grew ΔL^*, then the leftover increment $(\Delta L^* - Ld + Lc)$ was carried over to the next cell cycle. In these simulations, we kept a constant number of cells by simply choosing one daughter cell at each division to match the *DR* required. In the case of asymmetric division (*C. crescentus*), this corresponded to following the lineages of the longer progeny (stalked cell). In the modification where only one event X was allowed per division cycle, any extra events X were postponed until after the next division event. Furthermore, if no event X happened between two consecutive divisions, then event X was forced to happen at the second division.

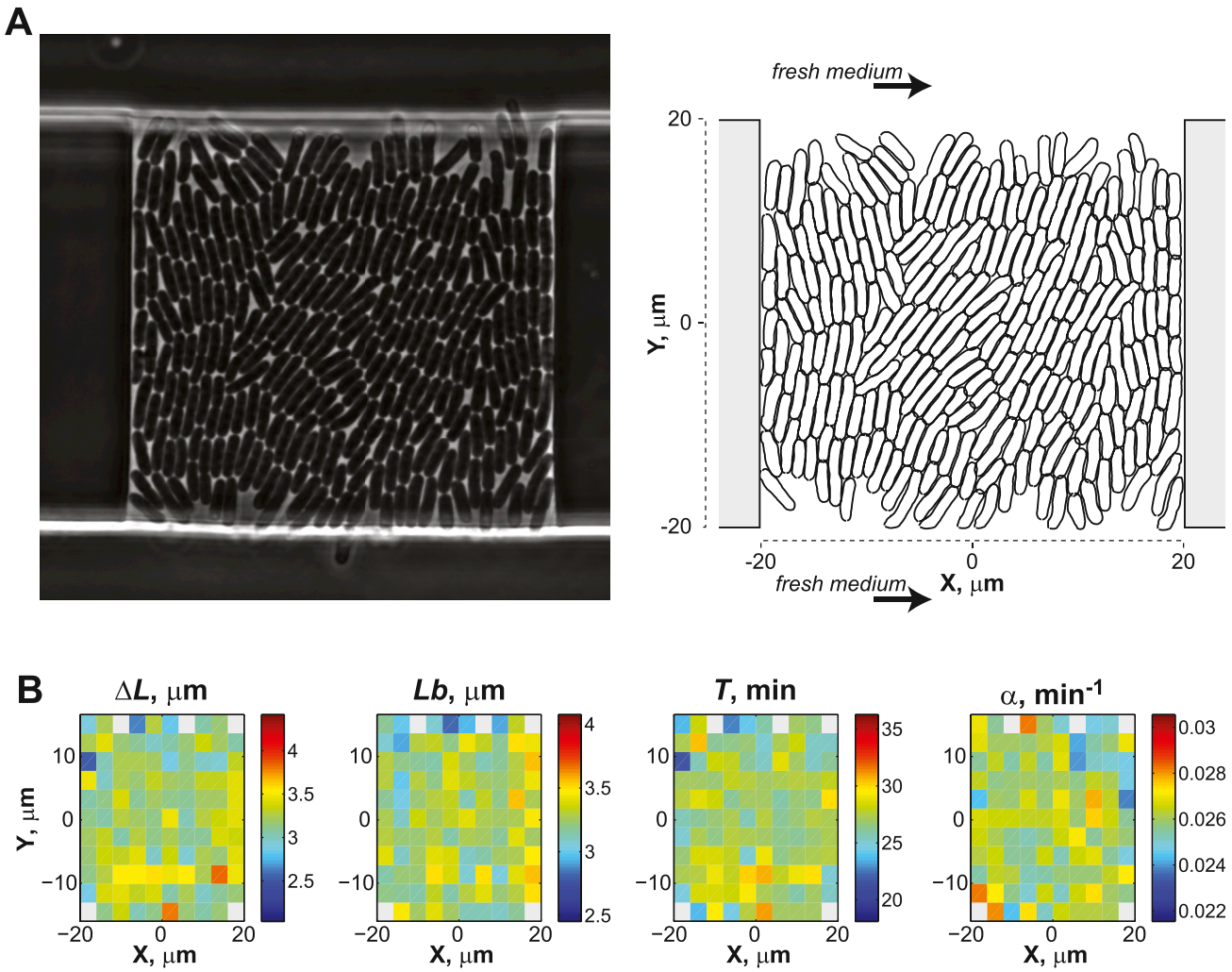

Figure S1. *E. coli* Cells Experience the Same Environment over the Entire Microfluidic Chamber, Related to Figure 2

(A) Image (left) and schematic (right) of one chamber filled with *E. coli* BW25113 cells growing in LB medium. The dimensions of the chamber and the flow of the medium are indicated by the broken lines and bold arrows, respectively.

(B) Two-dimensional histograms (shown as a heat map) for the elongation ΔL, the length at birth Lb, the cell cycle time T, and the elongation rate α as a function of the position of each cell in the chamber at the time of division. The color scales are centered on the mean ± 2 standard deviations for each variable. This interval encompasses ~95% of the cells (n = 1,305). The gray color on the heat maps indicates an area of the chamber at which no cell has divided during the course of the experiment.

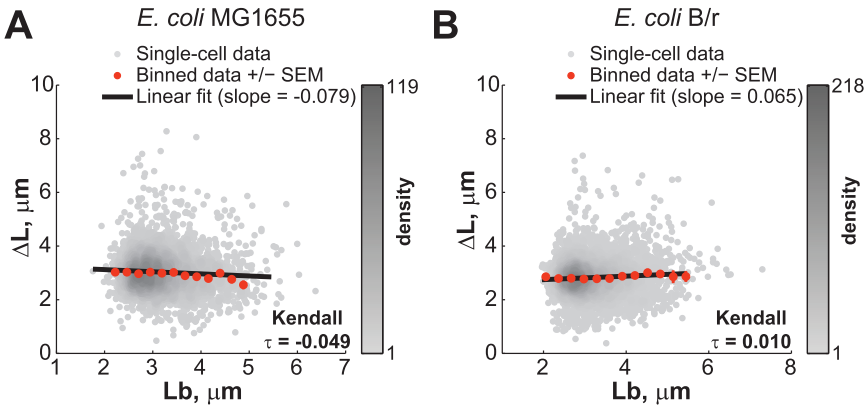

Figure S2. ΔL and Lb Are Independent for Other *E. coli* Strains Grown at 37°C, Related to Figure 2

(A) Relationship between *ΔL* and *Lb* for *E. coli* MG1655 cells (n = 4,612) grown in LB medium at 37°C. The raw data were obtained from Wang et al. (2010) via http://jun.ucsd.edu/mother_machine.php. The black line represents the linear fit to single-cell data.

(B) Same as (A) but for *E. coli* B/r cells (n = 7,620).

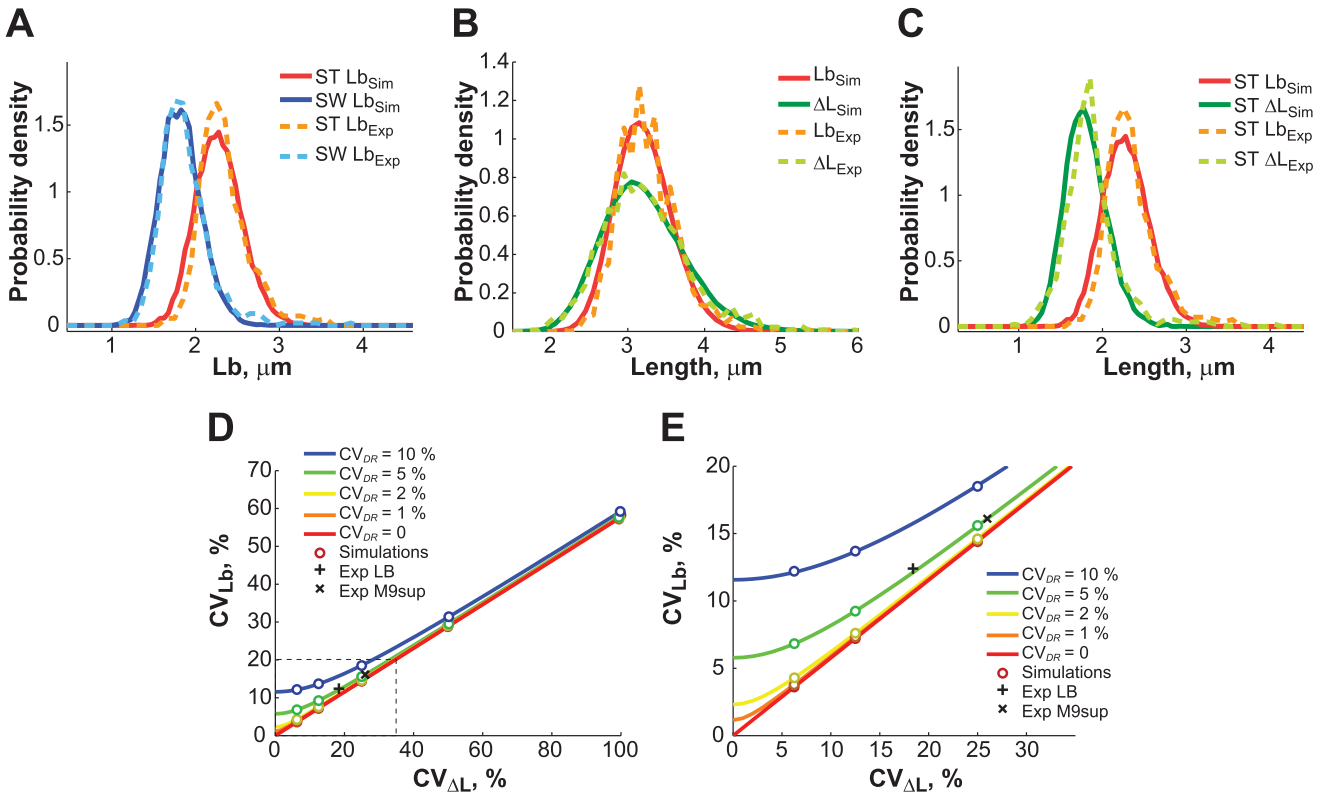

Figure S3. Analysis of Experimental Distributions, Related to Figure 3

(A) Plot showing the *Lb* distributions for *C. crescentus* stalked and swarmer cells from experiments and simulations.

(B) Comparison between the simulated and experimental *Lb* and *ΔL* distributions for *E. coli* BW25113 cells (LB data set).

(C) Comparison between the simulated and experimental *Lb* and *ΔL* of *C. crescentus* CB15N cells.

(D) Dependence of the CV of the length at birth (CV_{Lb}) with the CV of the elongation ($CV_{\Delta L}$) for different values of the CV of the division ratio (CV_{DR}). The lines represent the theoretical dependence from the constant extension model (see SI, Equation 15 for the analytical expression) while the circles represent the result of the simulations. The experimental results are displayed as black crosses.

(E) Magnified view of the area boxed in dashed lines in (D).

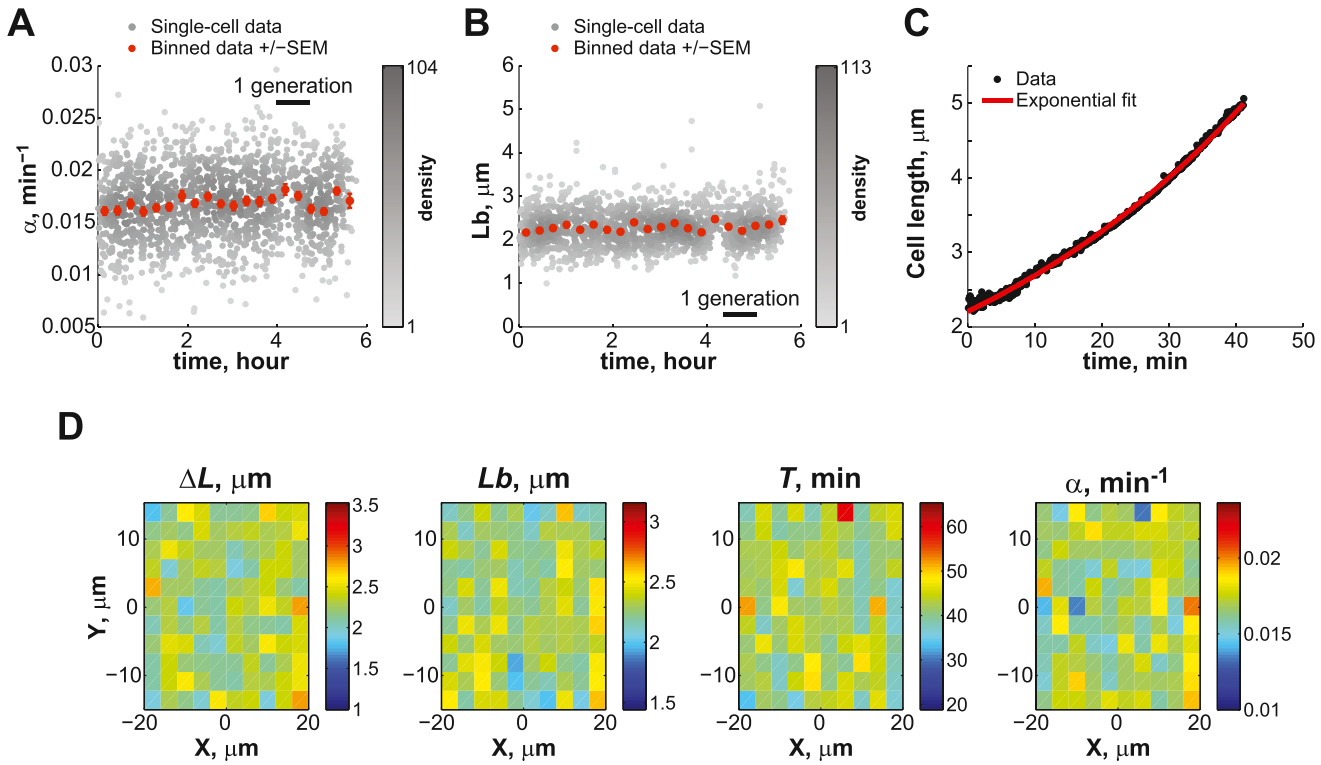

Figure S4. Homogeneous and Steady-State Growth of *E. coli* Cells in Microfluidic Chambers with M9-Supplemented Medium, Related to Figure 5

(A) Maintenance of a stable growth rate α over the course of the 6h-long experiment (n = 1,528 cells).

(B) Same as (A) but for *Lb* (n = 1,528 cells).

(C) Representative growth curve of a single cell (black circles). Length was measured every 5 s. The data were fitted by an exponential function represented by the red line.

(D) Two-dimensional histograms (shown as a heat map) of ΔL, *Lb*, the cell cycle time *T* and α as a function of each cell position at division. The color scales are centered on the mean ± 2 standard deviations for each variable. This interval encompasses ~95% of the cells.

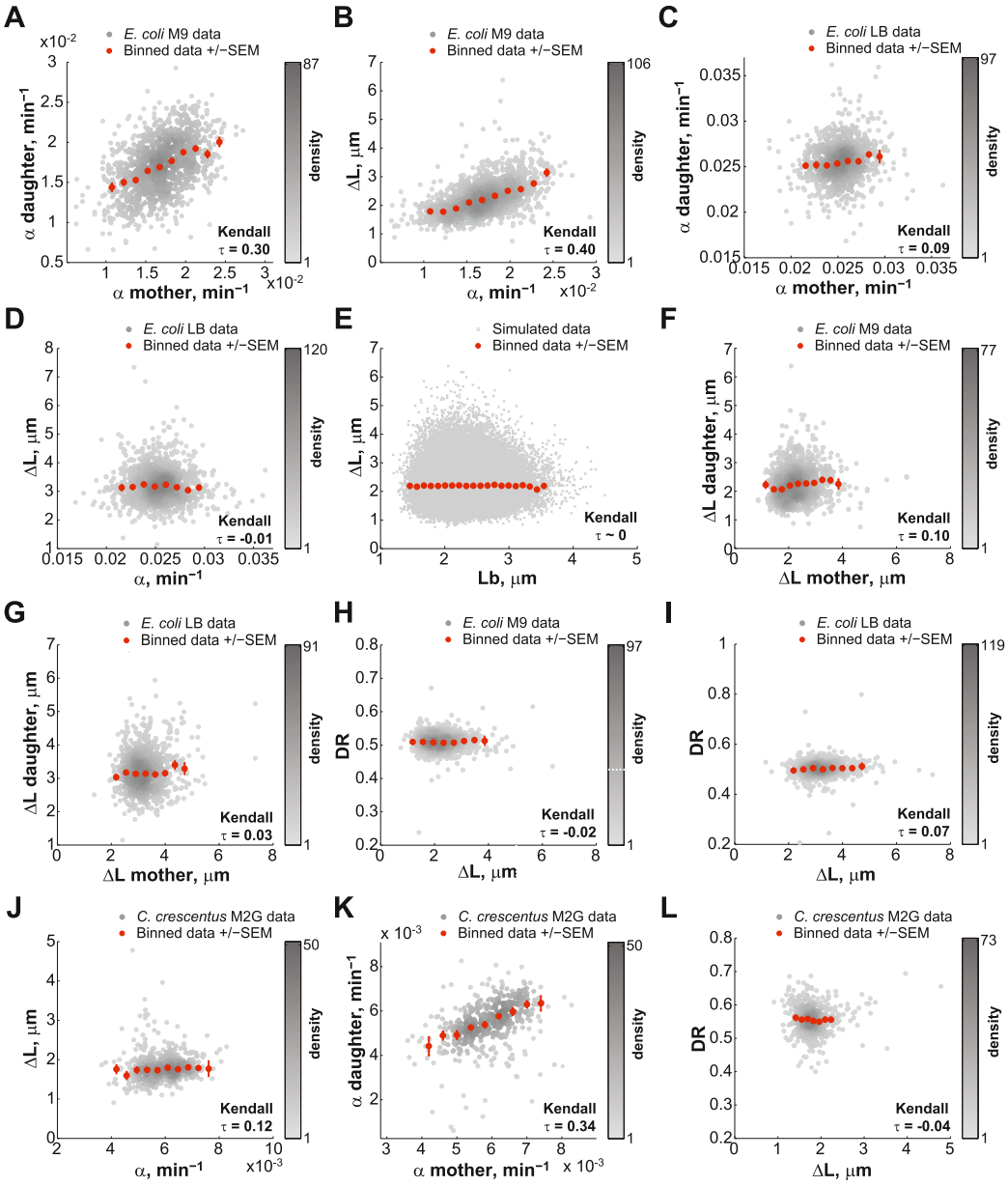

Figure S5. Correlations between Various Parameters for the *E. coli* and *C. crescentus* Data Sets, Related to Figures 1, 2, 3, and 5

For *E. coli* BW25113 cells grown in microfluidic chambers:

(A) Degree of inheritance of α over one generation in M9 supplemented medium (n = 1,203 cells).

(B) Dependence of *ΔL* on α in M9 supplemented medium(n = 1,528 cells).

(C) Degree of inheritance of α over one generation in LB medium (n = 1,025 cells).

(D) Dependence of *ΔL* on α in LB medium (n = 1,305 cells).

(E) Plot showing the simulated dependence of *Lb* and *ΔL* when the levels of correlation shown in (A) and (B) are taken into account (n > 60,000 virtual cells).

(F) Degree of inheritance of *ΔL* over one generation (n = 1,203 cells) in M9 supplemented medium.

(G) Degree of inheritance of *ΔL* over one generation in LB medium (n = 1,025 cells).

(H) Dependence of *DR* on *ΔL* in M9 suppelemented medium (n = 1,528 cells).

(I) Dependence of *DR* on *ΔL* in LB medium(n = 1,305 cells).

For *C. crescentus* grown on M2G soft-agar pads:

(J) Dependence of *ΔL* on α (n = 565 cells).

(K) Degree of inheritance of α over one generation (n = 457 cells).

(L) Dependence of *DR* on *ΔL* (n = 565 cells).

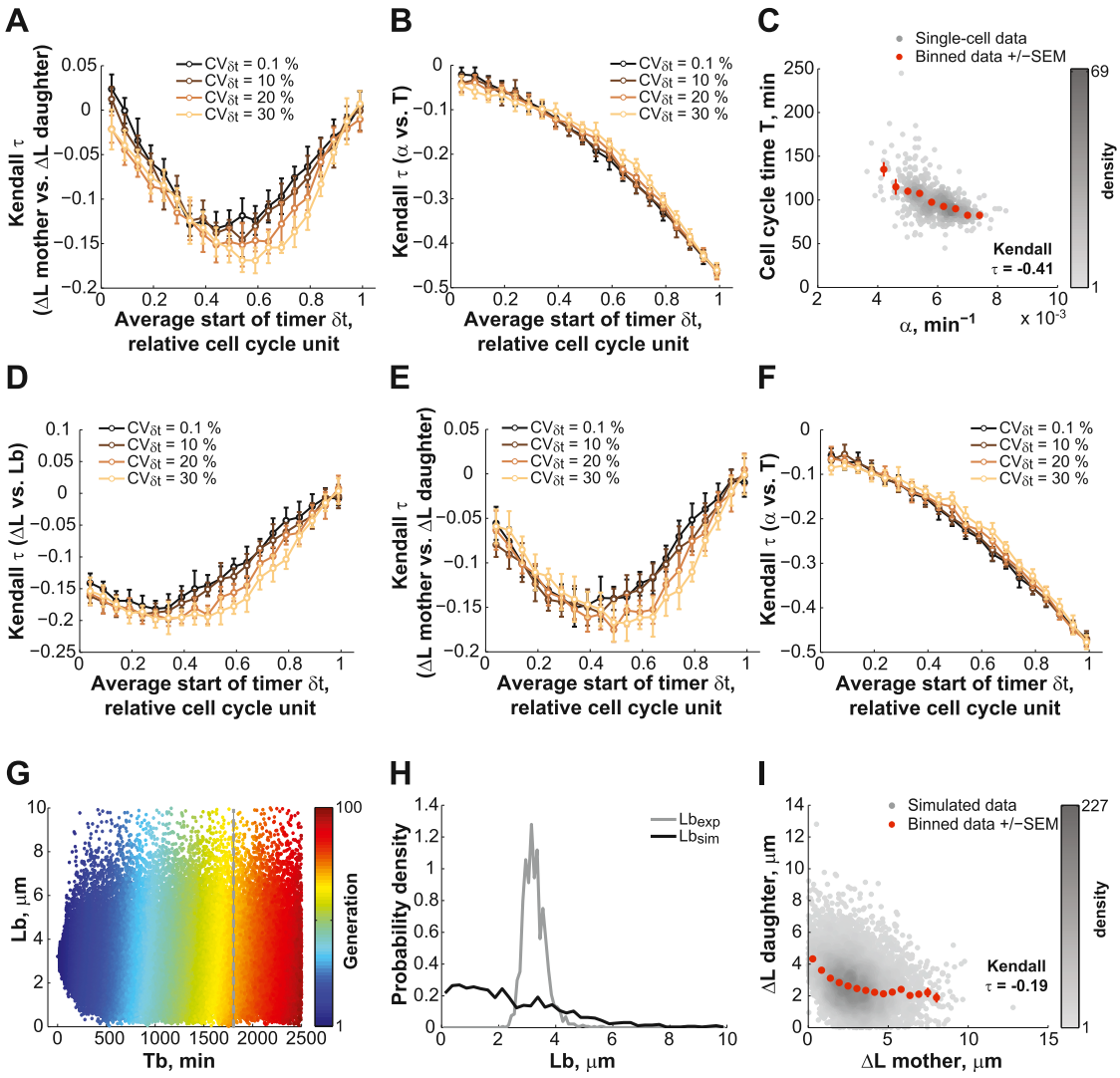

Figure S6. Phase-Shifted Constant Extension Model Coupled to a Timer Longer Than the Interdivision Time, Related to Figure 6

We simulated the phase-shifted model applied to a cell cycle event X coupled to division through a timer $\delta t > T$ (see SI and Table S1).

(A) Kendall correlation coefficients for ΔL between mother and daughter cells as a function of the timer starting time. *DR* was 0.56 to reflect the experimental division ratio for *C. crescentus*. The error bars shows the standard deviation obtained from 10 simulations performed with 1,500 cells.

(B) Kendall correlation coefficients between α and *T* as a function of the timer starting time. *DR* = 0.56.

(C) Scatter plot illustrating the experimental dependence of *T* on α for *C. crescentus* stalked cells (n = 457 cells).

(D) Same plot as Figure 6D for *DR* = 0.5.

(E and F) are the same plots as panels A and B, respectively, for *DR* = 0.5.

(G) Plot showing *Lb* versus time at birth (*Tb*) for simulations of the phase-shifted model with $\delta t > T$.

(H) Plot showing the *Lb* distribution at the time indicated by the dashed line in (G) compared to the experimental distribution.

(I) Plot showing the correlation between ΔL (from birth to division) of mother and daughter cells in data obtained from simulations of a phase-shifted model with $\delta t > T$ and with the extra requirement that the cell cycle event X occurs only once per division cycle (see SI and Table S1).

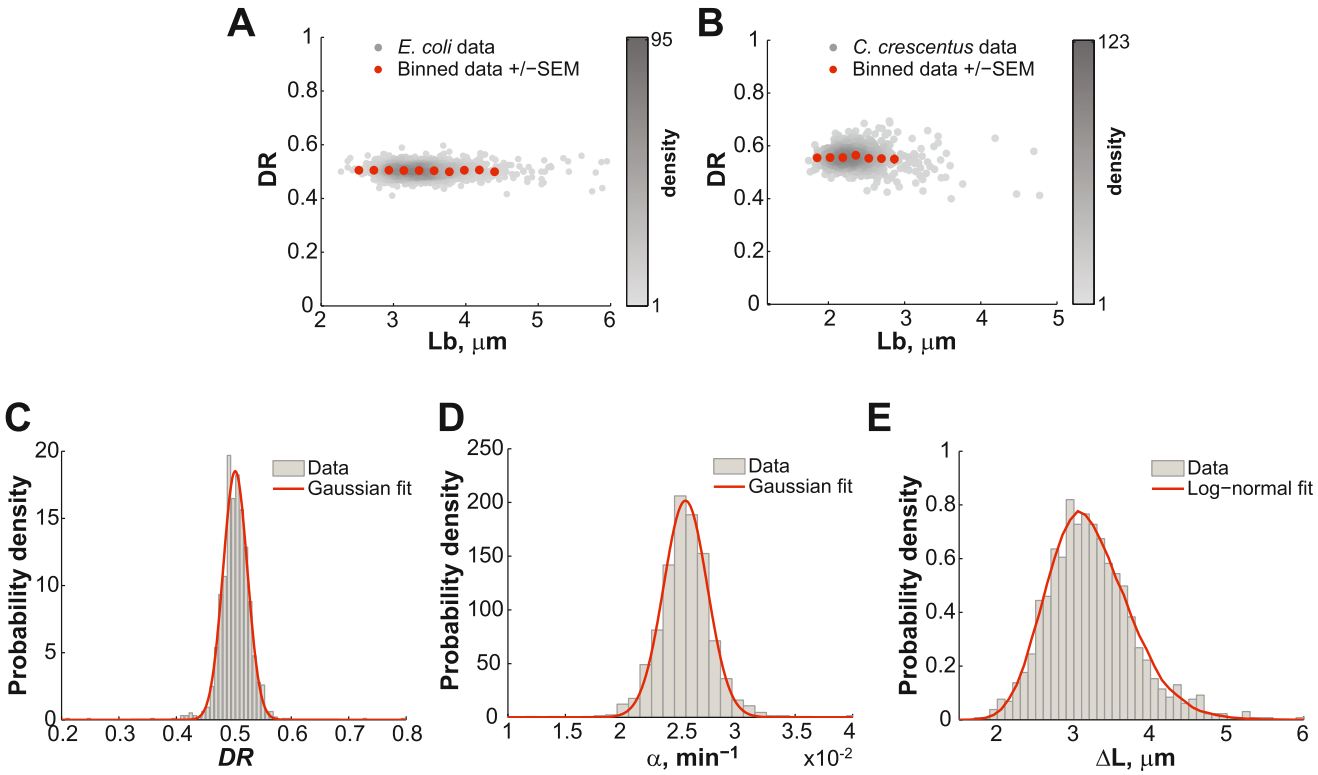

Figure S7. Analysis of Experimental Distributions and Relationships, Related to Figures 1 and 2

(A–D) Results from *E. coli* BW25113 cells (n = 1,305) grown in microfluidic chambers at 30°C in LB medium. (A) The experimental distribution of ΔL is consistent with a log-normal distribution. (B) The experimental distribution of *DR* appears Gaussian. (C) The relative growth rate α distribution was also well fitted by a Gaussian. (D) Relationship between *DR* and *Lb*.

(E) Same as (D) but for *C. crescentus* stalked cells (n = 565) grown at 30°C in M2G medium on 0.3% agarose pads.